AD_____

Award Number: W81XWH-11-1-0270

TITLE: Enhancement of Radiation Therapy in Prostate Cancer by DNA-PKcs Inhibitor

PRINCIPAL INVESTIGATOR: Debabrata Saha, Ph.D.

CONTRACTING ORGANIZATION: University of Texas Southwestern Medical Center
Dallas, TX 75390-7208

REPORT DATE: SEPTEMER 2014

TYPE OF REPORT: FINAL

PREPARED FOR: U.S. Army Medical Research and Materiel Command
Fort Detrick, Maryland 21702-5012

REPORT DOCUMENTATION PAGE

Form Approved
OMB No. 0704-0188

1. REPORT DATE	2. REPORT TYPE	3. DATES COVERED
SEPTEMBER 2014	FINAL	1 July 2011 – 30 June 2014

4. TITLE AND SUBTITLE

Enhancement of Radiation Therapy in Prostate Cancer by DNA-PKcs Inhibitor

5a. CONTRACT NUMBER

5b. GRANT NUMBER
W81XWH-11-1-0270

5c. PROGRAM ELEMENT NUMBER

6. AUTHOR(S)

Debabrata Saha, Ph.D.

E-Mail: Debabrata.Saha@utsouthwestern.edu

5d. PROJECT NUMBER

5e. TASK NUMBER

5f. WORK UNIT NUMBER

7. PERFORMING ORGANIZATION NAME(S) AND ADDRESS(ES)

University of Texas Southwestern Medical Center
Dallas, TX 75390-7208

8. PERFORMING ORGANIZATION REPORT NUMBER

9. SPONSORING / MONITORING AGENCY NAME(S) AND ADDRESS(ES)
U.S. Army Medical Research and Materiel Command
Fort Detrick, Maryland 21702-5012

10. SPONSOR/MONITOR'S ACRONYM(S)

11. SPONSOR/MONITOR'S REPORT NUMBER(S)

12. DISTRIBUTION / AVAILABILITY STATEMENT
Approved for Public Release; Distribution Unlimited

13. SUPPLEMENTARY NOTES

14. ABSTRACT

Prostate cancer (PCa) is the second leading cause of cancer death (~30,000/year) in men in the USA. Surgery and radiotherapy are the most effective therapies to treat PCa patients. However, both these forms of treatment, show significant tumor recurrence with locally aggressive disease, metastasis and the morbidity in patients. Several biological disorders are thought to underlie the cause of prostate cancer. One such factor is a tumor suppressor gene DAB2IP which encodes a member of the Ras-GAP protein family. Genome wide Single Nucleotide Polymorphism (SNP) association studies in a large number of patients indicated that DAB2IP is linked with the risk of aggressive prostate cancer. DAB2IP deficient PCa cells are resistant to radiation treatment. Therefore, to improve radiation killing of these aggressive PCa cells, this proposal will explore the radiosensitizing property of NU7441, a specific kinase inhibitor of DNA-PKcs.

15. SUBJECT TERMS
Radiation therapy, Prostate cancer, Radio-sensitization, DNA-Double strand break, cell cycle

16. SECURITY CLASSIFICATION OF:			17. LIMITATION OF ABSTRACT	18. NUMBER OF PAGES	19a. NAME OF RESPONSIBLE PERSON
a. REPORT	b. ABSTRACT	c. THIS PAGE			USAMRMC
U	U	U	UU	45	19b. TELEPHONE NUMBER *(include area code)*

Table of contents

Introduction

Prostate cancer (PCa) is the second leading cause of cancer death (~30,000/year) in men in the USA. Surgery and radiotherapy are the most effective therapies to treat PCa patients. However, both these forms of treatment, show significant tumor recurrence with locally aggressive disease, metastasis and the morbidity in patients. Several biological disorders are thought to underlie the cause of prostate cancer. One such factor is a tumor suppressor gene DAB2IP which encodes a member of the Ras-GAP protein family. Genome wide Single Nucleotide Polymorphism (SNP) association studies in a large number of patients indicated that DAB2IP is linked with the risk of aggressive prostate cancer. DAB2IP deficient PCa cells are resistant to radiation treatment. Therefore, to improve radiation killing of these aggressive PCa cells, this proposal will explore the radiosensitizing property of NU7441, a specific kinase inhibitor of DNA-PKcs. Three specific aims were proposed:

Aim 1: To test whether a DNA-PKcs inhibitor can radio-sensitize DAB2IP deficient aggressive PCa cells under normoxic and hypoxic conditions.

Aim 2: To study the role of DNA-PKcs in HIF-1α stabilization under hypoxic conditions in DAB2IP deficient prostate cancer cells.

Aim 3: To investigate the combined effect of a DNA-PK inhibitor and radiation therapy in a rodent orthotopic (OT) PCa model using image guided radiation therapy (IGRT).

Body:

Following tasks were proposed for the Year 3.

Task 9 (Specific Aim 3.1): Months 22-30
We will investigate the effect NU7441 in combination with radiation in rat orthotopic model. We like to start all the in vivo experiments at the same time in order to minimize the animal usage. Appropriate animals groups will be formed after implanting the DAB2IP deficient prostate cells as mentioned in experimental methods. Dr. Mathur who is an expert in ultrasound guided tumor cell implantation in the rat prostate will lead this study. He along with Dr. Song will perform the image guided radiation into the prostate. Dr. Song will be responsible for treatment planning, dosimetry, dose distribution and he will work under the supervision of Dr. Solberg. Dr. Mathur will administer the drug (NU7441) prior to radiation. After the treatment, Dr. Mathur will measure tumor volume using the ultrasound system and monitor tumor progression and metastasis by bioluminescence imaging. This task will be monitored very closely by Drs. Saha, Mathur, Song and Solberg. The reason this task takes a long time because we are anticipating a significant tumor growth delay in response to combined modality treatment. Statistical analysis will be performed by the Statistician Dr. Xie at our Simmons Cancer Statistical Core.

Task 10 (Specific Aim 3.2): Months 31-33
We will perform immunohistological analysis of the rat prostate tumors to evaluate the combined modality treatment efficacy. Tumor samples will be assessed for HIF-1α expression for elevated transcriptional activity, Ki67 expression for proliferation TUNEL assays for apotosis, γH2AX staining For DNA damage/repair response and hypoxic region by pimonidazole staining. Samples will be collected from a groups as mentioned in Aim 3.1, however, a smaller # rats will be used for each group (n=3). Radiation and the imaging will be performed by Dr. Song; while Drs. Mathur, Lin and Ms. Gore will perform the IHC.

Task 11 (Specific Aim 3.3): Months 33-35
Under this task we will analyze the potential damage to the bladder and rectum from radiation and radiation +Nu7441. Samples will be collected from the experiments as described in Aim 3.2. Damage to the rectum and bladder will be evaluated histologically and these stained slides will be evaluated on a scale of 0 to 4 by Dr. Payal Kapur, the pathologist in the department of Pathology at UTSouthwestern Medical Center (Letter of Collaboration attached). Similarly, staining will be performed by Dr. Mathur and Ms.Gore.

Task 12 (progress report and manuscript preparation): Months 35-36
Dr. Saha will prepare the annual report on the 3rd year progress and the comprehensive project report for the last 3 years developments and novel findings. He will also prepare manuscript focusing on the efficacy of combined modality therapy of radiation and NU7441 in highly aggressive DAB2IP deficient prostate cancer cell. Drs. Saha, Chen, Kapur and Hsieh will closely work on the preparation of the manuscript.

Key Research Accomplishment:

Continuation of Task 7:

Last year we mentioned under Task 7 "Our original finding of DNA-PKcs's role on HIF-1α stability under hypoxic condition was observed in HCT116 cells, therefore, we proposed to perform similar studies in prostate cancer cells after knocking down DNA-PKcs. However, our results in C4-2 Neo and C4-2 D2 cells showed that the stability of HIF-1α is not completely dependent on DNA-PKcs. As shown above, that in multiple experiments using specific DNA-PKcs inhibitors, we were unable to demonstrate HIF- 1α destabilization as we have seen in HCT116 cells. Therefore, the mechanism of HIF-1α regulation is different in various cancer types. We also studied in other PCa cell lines (PC3 and DU145) but no appreciable change was noticed. We perform luciferase assays as proposed in Task 7 and the results were shown in previous section. Therefore, to perform further experiments as proposed in task 7 will not be helpful". We also reported last year that while studying the regulation of HIF-1α in PCa cells, we noticed that DAB2IP could be phosphorylated during mitosis and showed evidence to that DAB2IP might be required for the release of checkpoint inhibition of APC/C and probably functions downstream of the kinetochore pathway which is an important mechanism of cellular aneuploidy. We continued working on this area under task 7 and made further progress.

Here, we found that DAB2IP localized at kinetochore during mitosis (Figure 1, Panel A). The inhibition of APC/C-CDC20 complex play pivotal role in SAC maintenance, therefore, we detected whether the DAB2IP could interact with APC/C-CDC20 complex. We found that both of CDC20 and Cdc27 could co-precipitate with DAB2IP during mitosis. We further defined the regions of DAB2IP that was required for their interaction, and found that the CPR region (amino acids 522-807) of DAB2IP was indispensable for the association between DAB2IP and CDC20 (Figure 1, B and C).

DAB2IP interacts with CDC20

Figure 1

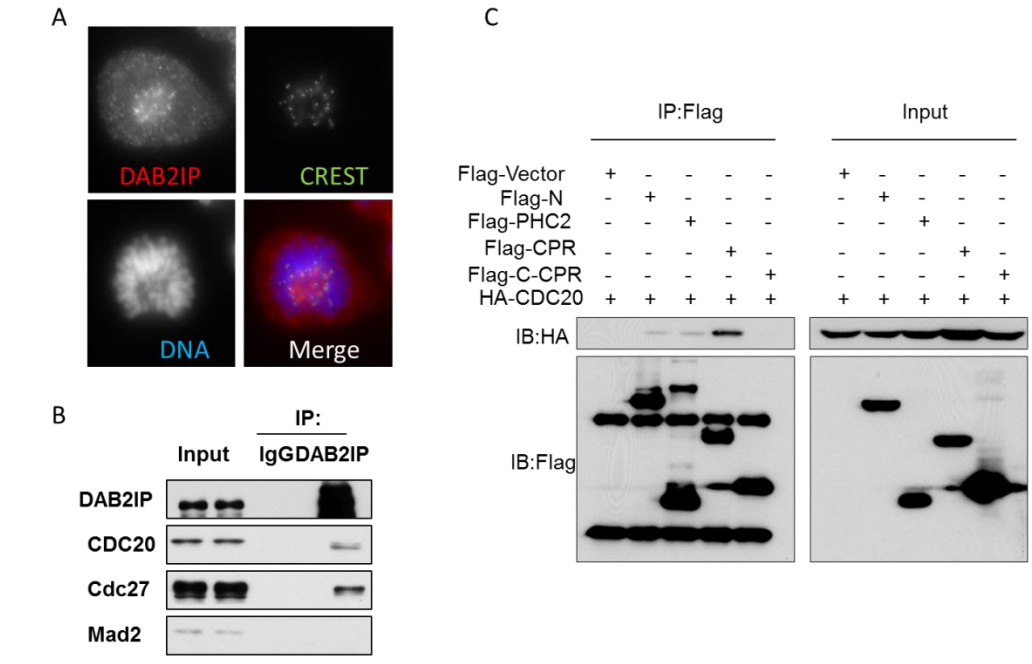

Figure 1. DAB2IP interacts with CDC20. (A) IF staining showed that DAB2IP overlaps with kinetochore marker crest during mitosis. (B) IP experiment revealed that DAB2IP could interact with CDC20 and Cdc27. (C) Immunoassay of 293T cells co-transfected with vectors expressing HA-tagged Cdc20 and Flag-tagged deletion mutants of DAB2IP; cells were treated with nocodazole, lysates were immunoprecipitated with anti-Flag M2 beads and immunoprecipitates were probed with an anti-HA or anti-Flag antibody

DAB2IP is required for the maintenance of MCC-APC/C complex during prometaphase in the presence of active checkpoint:

The disassociation of Mad2 and BubR1 from APC/C is necessary for APC/C-CDC20 activation and SAC sacrifice. We next investigated whether DAB2IP might alter the APC/C function by affecting the steady-state levels of these proteins on APC/C. Immunobloting analyses revealed that DAB2IP lead to accumulation of MCC on the APC/C. We synchronized the cells in prometaphase using nocodazole, and then release the cells into nocodazole free media to observe whether DAB2IP regulated the disassociation of Mad2 from APC/C. In DAB2IP proficient cells, the interaction of Mad2 with CDC20 was greatly stabilized following release from nocodazole arrest. Therefore, these results in Figure 2 (A, B and C) indicated that DAB2IP was critical for APC/C-MCC complex maintenance.

Figure 2

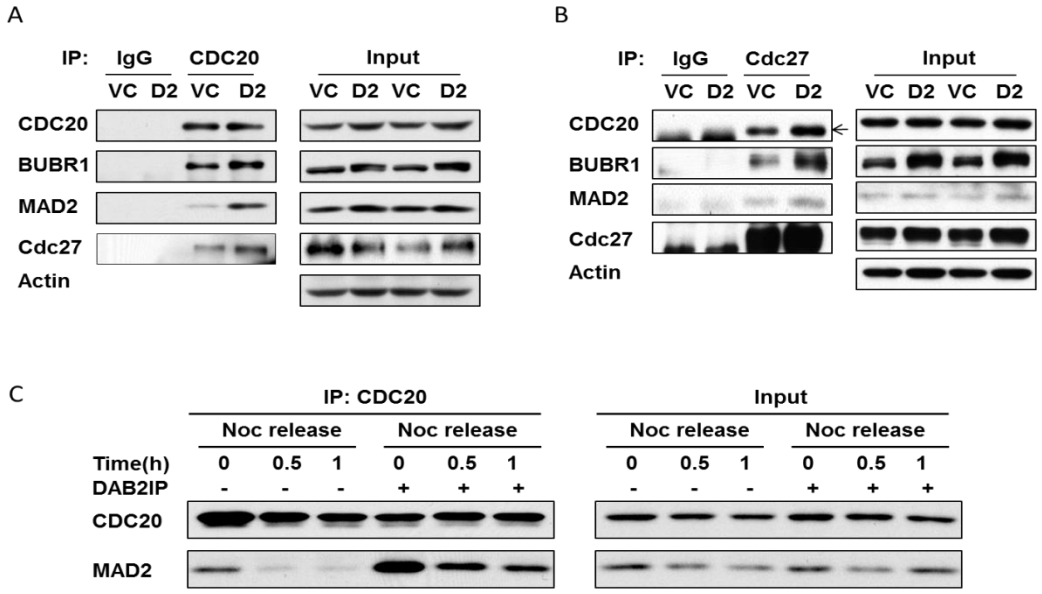

Figure 2. DAB2IP is required for the maintenance of MCC-APC/C complex during prometaphase in the presence of active checkpoint. (A, B) Anti-CDC20 and anti-Cdc27immunoprecipitated (IP) from DAB2IP proficient- and deficient- C4-2 cells arrested in prometaphase were analysed by immunoblotting. (C) CDC20 was immunoprecipitated (IP) at the indicated times after nocodazole washout. The amounts of co-precipitated Mad2 were visualized by western blotting (upper panel). Whole-cell lysates were analysed by immunoblotting with indicated antibodies (lower panel).

CDC20 turnover in prometaphase is prolonged by DAB2IP:

Recently, several reports demonstrated that dynamic degradation of CDC20 during prometaphase is an efficient way to promote APC/C-MCC complex dissociation. Therefore, we analyzed whether DAB2IP might affect CDC20 stability. We synchronized the C4-2 cells in

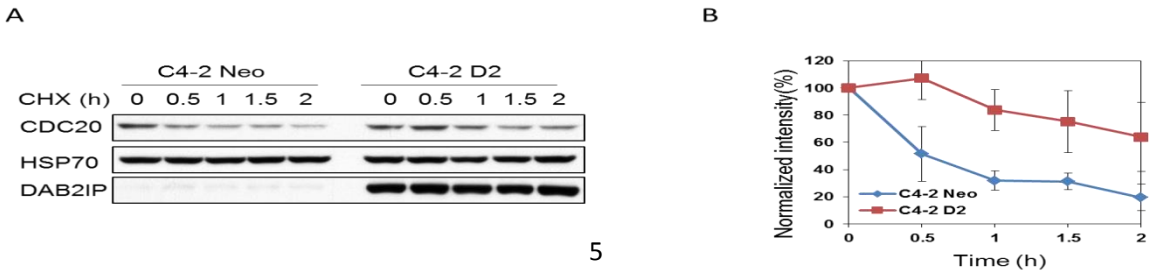

prometaphase and treated with cycloheximide for different time. Notably, the rate of this proteolysis was slowed down in DAB2IP proficient C4-2 cells (Figure 3).

Figure 3. CDC20 turnover in prometaphase is prolonged by DAB2IP. (A) Western blot showing CDC20 degradation in prometaphase-arrested control- and DAB2IP-expressed C4-2 cells; (B) Mean CDC20 protein levels in cycloheximide-treated control- and DAB2IP-overexpressed C4-2 cells.

DAB2IP is required for chromosome segregation and chromosomal stability maintenance:

The defect of SAC is one of the main reasons leading to chromosomal instability, which was a hallmarker and driving force for the tumor progression. We next detected whether the DAB2IP contributes to chromosomal stability maintenance. Firstly, we examined the chromosome movements in C4-2 cells through an unchallenged mitosis. We found that the percentage of cells with lagging chromosomes markedly decreased in DAB2IP-expressing cells. Using flow cytometry and chromosome spread methods, we also identified that DAB2IP could dramatically inhibited the increase of aneuploidy cells.

Figure 4

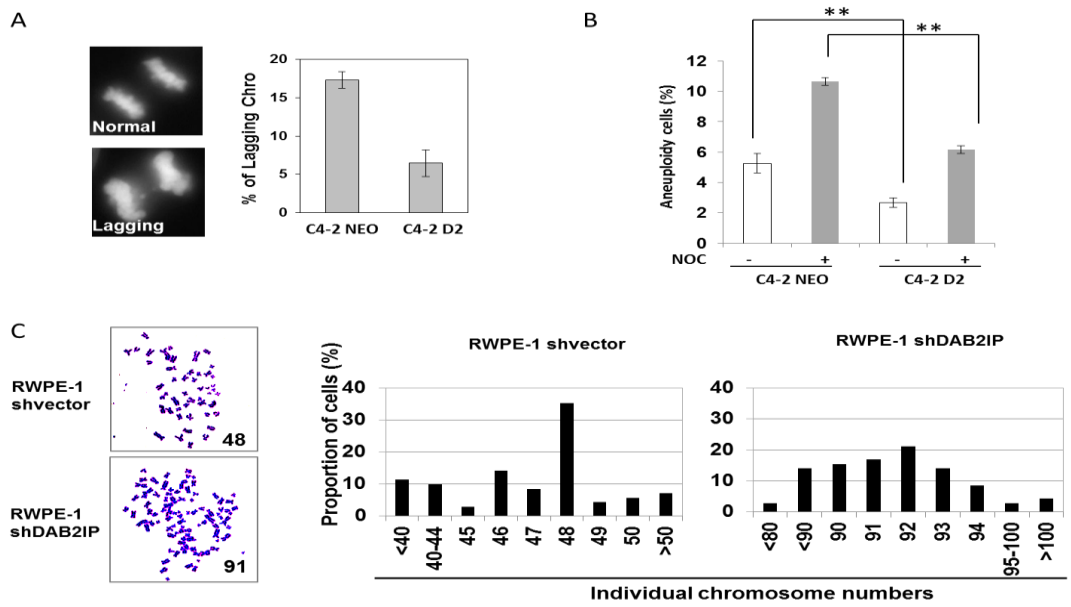

Figure 4. DAB2IP is required for chromosome segregation and chromosomal stability maintenance. (A) Analysis of chromosome-segregation defects in DAB2IP proficient- and deficient- C4-2 cells. Error bars, Data are representative of three independent experiments. Left side, representative images of normal and lagging chromosomes in C4-2 cells. (B) Flow cytometry analysis of aneuploidy cells in DAB2IP proficient- and deficient- C4-2 cells. (C) Quantification of the aneuploidy cells using chromosomal spread experiment.

Task 9 Continuation:

As mentioned in our last year's report, that we have already standardized the conditions to develop prostate orthotopic model in rats and published our findings in the ***Journal of International of Oncology***. However, we have encountered several problems that hindered the timely progress in finishing the specific aim 3 in a timely manner. Therefore, we have requested no cost extension and here is what we wrote in an email on May 23, 2014 to the members of the DOD PCRP "The results among the treatment groups are not consistent because of imaging issues. Since the primary readout is bioluminescence signal from the tumor produing cells and we have some problem with the optimal time of acquisition of the signal and the tumor growth. We found that problem is in the PCa cell lines which transfected with Luciferase cell line. Therefore, we are testeng the different clones of this recombinant cell before we implant into the animals. We are cofident that we will be able to finish all the proposed studies within the extended period as requested".

However we are continuing working on Task 9 and below are some of the results:
We implanted PC3KD-luc cells orthotopically inside the prostate of adult male nude rats and using ultrasound as the primary tumor measurement tool instead of BLI to monitor the tumor progression. Tumors were radiated with 3 fractions of 12 Gy. We found the irradiation (3 X 12Gy) had a significant impact on tumor growth (Figure 5, A-C).

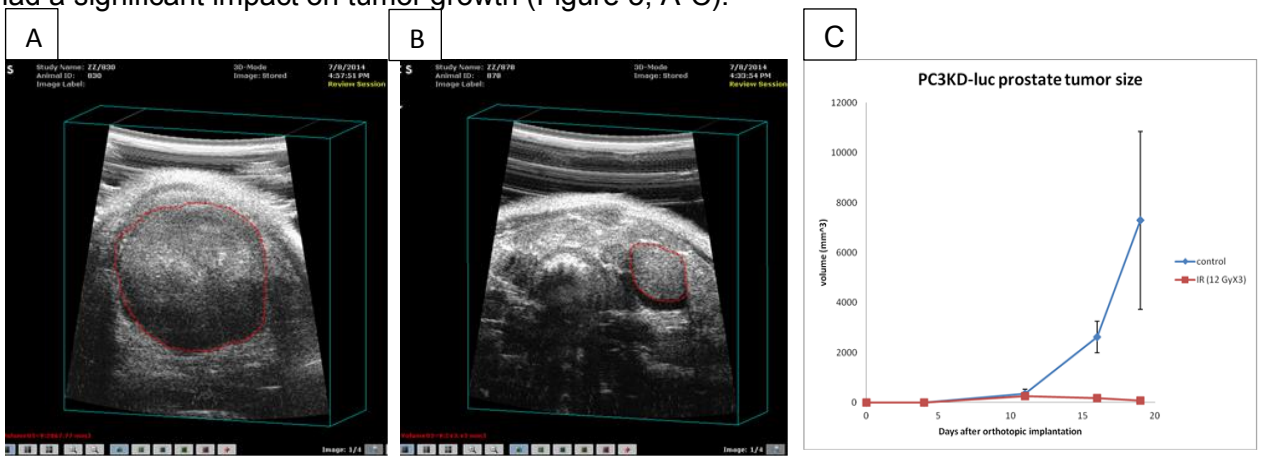

Figure 5: Prostate tumors measured by ultrasound. **A.** Control and **B**. Irradiation. **C**. Tumor progression curve.

We also observed the irradiation treatment of 3 X 12Gy causes GI tract toxicity as shown in Figure 6 in some animals. In order to minimize the toxicity of irradiation, we will combine the radiation treatment with NU7441 and will be performed during the extension period.

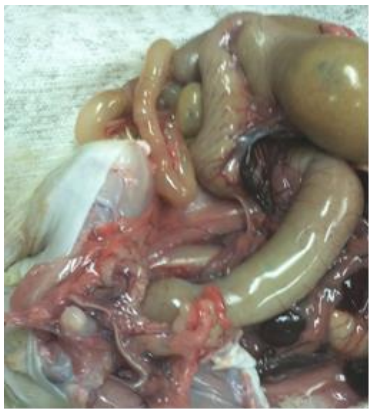

Figure 6. Rectum toxicity of irradiation. A blocked GI tract was discovered 4 weeks after dissecting a rat received irradiation (3 X 12Gy).

The work to be completed during the no cost extension period (Task 10 and 11):
Mostly the experiments proposed in the Aim 3 in the original proposal will be performed. Briefly; To determine the efficacy of the combined treatment, we will establish these groups (1) control, (2) radiation (12Gyx3), (3) radiation (12Gyx2), (4) radiation (12Gyx1), (5) NU7441 (25mg/kg), (6) NU7441+radiation (12Gyx3), (7) NU7441+radiation (12Gyx2), (8) NU7441+radiation (12Gyx2). We will measure the tumor volume using the Ultra Sound guided (USG) imaging and bioluminescence imaging (BLI). For Immunohistological analysis, we will establish similar animal groups and collect the tumor samples at different time points after treatment for (i) pimonidazole staining, (ii) HIF-1α expression level, (iii) Ki 67 staining (proliferation), (iv) γH2AX staining (For DNA damage/repair response) (v) DNA-PKcs staining (to differentiate normal and tumor tissue) and (v) Apoptosis Study. We will also analyze the radiation induced damage to the adjacent organs bladder and rectum by histology.

Task 12: This is our 3rd and final progress report. Currently, we are finalizing our manuscripts on the experiments performed under Task 7. We are expecting 2 manuscripts on these novel findings. So far we have published 4 articles in peer reviewed journals and 2 under preparation.

Reportable outcomes:

1. Recently we completed a pilot study to investigate the role of DAB2IP as prognostic biomarkers in high-risk prostate cancer patients receiving definitive radiation therapy. Fifty-four patients with high-risk prostate cancer (stage >T3a, or Gleason score >8, or prostate-specific antigen level >20 ng/mL) treated with radiation therapy from 2005 to 2012 at our institution were evaluated. This article is now published in the Journal of Int **J Radiation Oncol Biol Phys, Vol. 89, No. 4, pp. 729-735, 2014**. A copy of the article is attached

2. A multifunctional PLGA-based NPs were synthesized for sustained release of NU7441 for targeted radiosensitization of prostate cancer cells. To increase the target specificity of PLGA particles, the particles were further conjugated with R11-a polyarginine cell permeable peptide with prostate specificity, to form R11-NU7441 NPs. In this study, R11-conjugated PLGA-based NPs containing NU7441 were synthesized to selectively enhance the radiation sensitivity of prostate cancer cells. This study is now acceptable for publication in the **Journal of Biomedical Materials Research: Part A.** A copy of accepted Manuscript is attached.

3. In addition, Lan Yu will be presented an oral and poster on the role of DAB2IP in mitotic spindle assembly checkpoint (modified **Task 7)** at the Annual Radiation Research Society (RRS) Meeting in Las Vegas, September 2014. Dr. Yu is also received the Scholar in Training (SIT) award for her study from the RRS.

Conclusion:
We have made significant progress which we described under Task 7 and 9. We are highly hopeful to finish the remaining tasks in the extended time requested.

References: References are included in the attached manuscript.

International Journal of Radiation Oncology biology • physics

www.redjournal.org

Biology Contribution

DOC-2/DAB2 Interacting Protein Status in High-Risk Prostate Cancer Correlates With Outcome for Patients Treated With Radiation Therapy

Corbin Jacobs, BS,* Vasu Tumati, MD,* Payal Kapur, MD,† Jingsheng Yan, PhD,‡ David Hong, MD,* Manzerul Bhuiyan, MS,* Xian-Jin Xie, PhD,‡ David Pistenmaa, MD, PhD,*,§ Lan Yu, PhD,* Jer-Tsong Hsieh, PhD,§,|| Debabrata Saha, PhD,*,§ and D. W. Nathan Kim, MD, PhD*,§

*Departments of *Radiation Oncology, †Pathology, ‡Clinical Sciences, and ||Urology, University of Texas Southwestern Medical Center, Dallas, Texas; and §Simmons Cancer Center, Dallas, Texas*

Received Jan 23, 2014, and in revised form Mar 18, 2014. Accepted for publication Mar 21, 2014.

Summary

Our pilot study demonstrates that tumor DAB2IP status may predict outcome after definitive radiation therapy in high-risk prostate cancer patients, and the prognostic value may be improved by also measuring EZH2 intensity levels.

Purpose: This pilot study investigates the role of DOC-2/DAB2 Interacting Protein (DAB2IP) and enhancer of zeste homolog 2 (EZH2) as prognostic biomarkers in high-risk prostate cancer patients receiving definitive radiation therapy.

Methods and Materials: Immunohistochemistry was performed and scored by an expert genitourinary pathologist. Clinical endpoints evaluated were freedom from biochemical failure (FFBF), castration resistance–free survival (CRFS), and distant metastasis–free survival (DMFS). Log-rank test and Cox regression were used to determine significance of biomarker levels with clinical outcome.

Results: Fifty-four patients with high-risk prostate cancer (stage ≥T3a, or Gleason score ≥8, or prostate-specific antigen level ≥20 ng/mL) treated with radiation therapy from 2005 to 2012 at our institution were evaluated. Nearly all patients expressed EZH2 (98%), whereas 28% of patients revealed DAB2IP reduction and 72% retained DAB2IP. Median follow-up was 34.0 months for DAB2IP-reduced patients, 29.9 months for DAB2IP-retained patients, and 32.6 months in the EZH2 study. Reduction in DAB2IP portended worse outcome compared with DAB2IP-retained patients, including FFBF (4-year: 37% vs 89%, $P=.04$), CRFS (4-year: 50% vs 90%, $P=.02$), and DMFS (4-year: 36% vs 97%, $P=.05$). Stratified EZH2 expression trended toward significance for worse FFBF and CRFS ($P=.07$). Patients with reduced DAB2IP or highest-intensity EZH2 expression exhibited worse FFBF (4-year: 32% vs 95%, $P=.02$), CRFS (4-year: 28% vs 100%, $P<.01$), and DMFS (4-year: 39% vs 100%, $P=.04$) compared with the control group.

Reprint requests to: D. W. Nathan Kim, MD, PhD, University of Texas Southwestern Medical Center, Department of Radiation Oncology, 5801 Forest Park Rd, Dallas, TX 75390. Tel: (214) 645-7695; E-mail: Nathan.Kim@utsouthwestern.edu

Conflict of interest: none.

This work was supported in part by DOD grant W81XWH-11-1-0270(D.S.)

Int J Radiation Oncol Biol Phys, Vol. 89, No. 4, pp. 729–735, 2014
0360-3016/$ - see front matter
http://dx.doi.org/10.1016/j.ijrobp.2014.03.035

Conclusion: Loss of DAB2IP is a potent biomarker that portends worse outcome despite definitive radiation therapy for patients with high-risk prostate cancer. Enhancer of zeste homolog 2 is expressed in most high-risk tumors and is a less potent discriminator of outcome in this study. The DAB2IP status in combination with degree of EZH2 expression may be useful for determining patients with worse outcome within the high-risk prostate cancer population. © 2014 Elsevier Inc.

Introduction

Prostate cancer is the most common male malignancy in the United States, with 238,000 cases and 29,720 deaths expected in 2013 (1), of which 20 to 30% have high-risk features (2). For high-risk prostate cancer defined by the National Comprehensive Cancer Network as stage ≥cT3a, Gleason score ≥8, or prostate-specific antigen (PSA) ≥20 ng/mL, standard treatment guidelines include definitive radiation therapy with neoadjuvant, concurrent, and long-term androgen deprivation therapy in the United States (3). Despite standard therapy, long-term outcomes are suboptimal, with 5-year biochemical progression-free survival of 60% to 70% and 5-year overall survival of 75% to 85% (4-7).

Identification of patients who are most likely to have poor outcomes despite dose-escalated radiation therapy with long-term androgen deprivation can be challenging. Being able to predict the patients that portend worse outcome at the time of diagnosis may provide means to offer patients an alternative, more-effective therapy, possibly through the auspices of a clinical trial. Multiple biomarkers have been studied in the setting of high-risk prostate cancer (8, 9), and although some have shown much promise, routine use of such markers in clinical practice has been limited (10). Additional biomarkers that can readily identify patients most likely to fail conventional therapy are warranted, and investigations of the molecular pathway involved in this poor outcome may further lead to future therapeutic interventions.

DOC-2/DAB2 Interacting Protein (DAB2IP), a member of the Ras GTPase-Activating Proteins (RAS-GAP) family, is a novel tumor suppressor. Decreased expression of DAB2IP is often detected in prostate cancer cells, and this loss of DAB2IP is primarily due to altered epigenetic regulation of its promoter (11). A genome-wide screening of single nucleotide polymorphisms indicated that a genetic variant in DAB2IP is linked with aggressive prostate cancer (12). Furthermore, a population-based case−control study confirmed that DAB2IP was linked with an increased risk of aggressive prostate cancer (12). Immunohistochemistry analysis of more than 200 patients with prostate cancer by Min et al (13) clearly demonstrated the causal role of DAB2IP loss in prostate cancer progression. The aggressive nature of DAB2IP-deficient tumors is explained by recent cell culture model studies, which have found that loss of DAB2IP can lead to radiation resistance, increased DNA repair ability, and decreased apoptosis after radiation (14-16).

Enhancer of zeste homolog 2 (EZH2), the catalytic unit of the polycomb repressor complex, is often up-regulated in several cancers, including breast, lung, and prostate (17). Our data indicate that DAB2IP is an EZH2 target gene in prostate cancer (18). Overexpression of EZH2 has been shown to drive prostate cancer progression, and studies have shown that clinically localized tumors that express high levels of EZH2 have poorer outcomes (19, 20). Additionally, it has been shown that in low-risk tumors EZH2 expression has been correlated with poor surgical outcomes (19).

Although several cell culture and animal-based models have shown that DAB2IP and EZH2 are involved with increased radiation resistance (14, 15, 21), there is no study that evaluates the clinical relevance of DAB2IP-mediated radiation resistance. Therefore, we sought to determine the prognostic value of DAB2IP and its upstream regulator EZH2 in high-risk prostate cancer patients.

Methods and Materials

Patient selection

All patients with prostate cancer treated with external beam radiation at our institution between December 2005 and July 2012 were identified. Of the 658 patients identified, 138 patients met the National Comprehensive Cancer Network guidelines for high-risk classification (stage ≥T3a, or Gleason score ≥8, or PSA ≥20 ng/mL) and did not receive any surgical management. Patients who had metastases before initial radiation therapy were excluded from the study. All patients were treated definitively with external beam radiation therapy using a variety of techniques, including dynamic arc therapy; all patients were treated with a dose exceeding 72 Gy, and 80% were treated to 79.2 Gy. Of the 138 patients identified, only those patients who provided signed consent, who had preserved pretreatment prostate biopsy tissue available, and whose biopsies had a sufficient tumor sample available for analysis were included in the study.

Specimen characteristics, staining, and quantification

Diagnostic needle biopsies were mounted in paraffin, and 3- to 4-μm sections were prepared for standard hematoxylin and eosin staining. Standard immunohistochemistry

analysis was performed for DAP2IP and EZH2. Immunostain was performed using the Benchmark XT automated stainer (Ventana, Tuscan, AZ). Briefly, formalin-fixed, paraffin-embedded tissue microarray sections were cut at 3-4 μm and air-dried overnight. The sections were deparaffinized, rehydrated, subjected to heat-induced epitope retrieval, and then incubated with anti-EZH2 (clone: SP129, Ventana, prediluted) or anti-DAB2IP (22) (homegrown, 1:150) primary antibodies. The UltraView universal detection system (Ventana) was used for signal detection. The slides were developed using 3-3′-diaminobenzidine chromogen and counterstained with hematoxylin. Specific positive and negative (slides incubated without primary antibody) controls were used for each run of immunostains and checked for validation of the assay. Controls for anti-EZH2 antibody included tissue from prostate and breast adenocarcinoma and normal lymph node that are known to have high EZH2 expression. The anti-EZH2 protocol was standardized according to the directions in the package insert. This antibody is intended for in vitro diagnostic use. The protocol for anti-DAP2IP was performed as previously reported (22).

Tumor and benign prostate tissue stained with each marker were evaluated by an experienced genitourinary pathologist who was blinded to patient clinical information. Each case was evaluated for the extent (percentage of positive cells) and intensity of staining. The average intensity of positive tumor cells was given a grade (G) score: G0, none; G1, weak; G2, intermediate; and G3, strong. The DAB2IP positivity was evaluated as cytoplasmic expression; EZH2 was evaluated as nuclear pattern of expression. Compared with DAB2IP expression in the benign "control" prostate tissue surrounding the neoplastic cells, tumor DAB2IP status was categorized as retained (same or stronger expression) or reduced (weaker expression). Expression of EZH2 was scored as the product of percentage of cells staining and the intensity of staining.

Study design

The 3 primary clinical endpoints in this study were freedom from biochemical failure (FFBF), castration resistance–free survival (CRFS), and distant metastasis–free survival (DMFS). Freedom from biochemical failure was determined using the Phoenix definition, which denotes a PSA increase of $\geq$2.0 ng/mL above the nadir PSA level (23). Castration resistance–free survival was defined as $\geq$2 episodes of rising PSA while receiving standard hormone therapy in the setting of testosterone levels <50 ng/mL, or if patients were started on second-line therapy because first-line hormone therapy was deemed to have failed at the clinical oncologist's discretion. Distant metastasis–free survival was determined from clinical chart review documenting date of known metastasis by imaging. Time to each endpoint was calculated from the first day of radiation therapy.

Statistical analysis

In this study there were 2 main biomarkers: DAB2IP and EZH2. A 2-sided log-rank test with an overall sample size of 46 for DAB2IP and 48 for EZH2 achieves 80% power at a 0.025 significance level to detect a significant difference in 4-year FFBF rates between the 2 groups. The sample size estimation was conducted using the sample size software PASS 11(NCSS, Kaysville, Utah). Kaplan-Meier estimates and log-rank tests were computed to estimate the FFBF, CRFS, and DMFS. Univariate Cox regression analysis of T stage, N stage, highest Gleason score, pretreatment PSA level, percentage of positive biopsy cores, total radiation dose, hormone therapy, and duration of hormone therapy was performed. Finally, Fisher exact test was used to evaluate statistical differences among these factors according to the status of the tumor biomarkers.

Results

Fifty-four patients with high-risk prostate cancer treated with definitive radiation therapy from 2005 to 2012 met the inclusion criteria and were evaluated. The median age of patients used for analysis was 66 years. Twenty-eight percent of patients (13 of 46) revealed DAB2IP reduction, whereas 72% (33 of 46) retained DAB2IP. Nearly all patients expressed EZH2 (98%), and the intensity level was G0 in 1 (2%), G1 in 9 (19%), G2 in 29 (60%), and G3 in 9 (19%) patients. The median pretreatment PSA level was 14.8 ng/mL (range, 1.2-208.9 ng/mL). Gleason scores were 7 in 22% of patients and 8-10 in 78% of patients. Clinical T stage category was T1c in 19% of patients, T2a-c in 56% of patients, and T3a-b in 22% of patients. Table 1 displays a distribution of patient characteristics.

The median follow-up was 34.0 months (range, 6.7-76.1 months) for DAB2IP-reduced patients, 29.9 months (range, 6.1-84.6 months) for DAB2IP-retained patients, and 32.6 months (range, 2.8-84.6 months) for patients in the EZH2 study. In the DAB2IP study there was no statistically significant difference between use of hormone therapy (P = .55) or duration of hormone therapy (P = .63). Of the patients in the EZH2 study who received hormone therapy, there was no significant difference in duration (P = .81).

Interestingly, reduction of DAB2IP in patient's prostate cancer samples correlated strongly with several poor outcome measures. Reduction of DAB2IP portended a significantly lower FFBF (Fig. 1A; P = .04) and increased likelihood of progression to castration resistance (P = .017). Patients with reduced DAB2IP compared with patients retaining DAB2IP had a 4-year FFBF of 37% and 89%, respectively. The 4-year CRFS for DAB2IP-reduced patients was 50%, whereas the 4-year CRFS was 90% for DAB2IP-retained patients. Loss of DAB2IP was not a statistically significant predictor of increased distant metastasis (P = .05), although it trended toward

Table 1 Patient characteristics compared with respect to major prognostic variables

Age (y), median (range)	66 (48-84)
T stage	
T1c	18.5 (10)
T2a-b	35.2 (19)
T2c	20.4 (11)
T3a	14.8 (8)
T3b	7.4 (4)
Unknown	3.7 (2)
N stage	
N0	90.7 (49)
N1	9.3 (5)
Pretreatment PSA level (ng/mL)	
<10	37.0 (20)
10-20	18.5 (10)
>20	44.4 (24)
Gleason score	
7	22.2 (12)
8	35.2 (19)
9	33.3 (18)
10	9.3 (5)
Total radiation dose (Gy)	
72-75.6	20.4 (11)
79.2	79.6 (43)
Hormone therapy	
Yes	92.6 (50)
No	7.4 (4)
Duration of hormone therapy (mo)	
0	7.4 (4)
4-18	35.2 (19)
24-36	57.4 (31)
Tumor DAB2IP status (n=46)	
Reduced	28.3 (13)
Retained	71.7 (33)
Tumor EZH2 status (n=48)	
Grade 0	2.1 (1)
Grade 1	18.8 (9)
Grade 2	60.4 (29)
Grade 3	18.8 (9)

Abbreviations: DAB2IP = DOC-2/DAB2 Interacting Protein; EZH2 = enhancer of zeste homolog 2; PSA = prostate-specific antigen.
Values are percentage (number) unless otherwise noted.

significance. Increased follow-up or a larger data set will most likely result in a significant outcome. The 4-year DMFS was 36% for DAB2IP-reduced patients and 97% for DAB2IP-retained patients. Median time to biochemical failure was 29.7 months and 23.7 months for the DAB2IP-retained and -reduced groups, respectively. The median time to castration resistance was 29.9 months and 27.6 months, whereas the median time to distant failure was 29.9 months and 26.7 months for the DAB2IP-retained and -reduced groups, respectively.

Analysis of EZH2 samples shows that nearly all high-risk patients exhibit expression of EZH2 (98%). Stratification of EZH2 expression was not significantly predictive of decreased FFBF (Fig. 1B; $P=.07$), increased castration resistance ($P=.07$), or decreased distant metastasis rate ($P=.2$), although it trended toward significance.

It is interesting to note, however, that combining patients who had either EZH2 G3 staining or decreased DAB2IP levels created a group found to have significantly worse outcomes. The 4-year FFBF for this combined group compared with the control group (retained DAB2IP and EZH2 G0-G2) was 32% versus 95% (Fig. 1C; $P=.0153$), the 4-year CRFS was 28% versus 100% ($P=.0019$), and the 4-year DMFS was 39% versus 100% ($P=.04$), respectively. Additionally, the combined group of DAB2IP-reduced or EZH2 G3 patients accounted for 6 of the 7 patients (86%) who were identified to have clinical castration resistance. Table 2 summarizes all patient outcomes by tumor biomarker status.

Of the 7 patients with castration resistance, their initial androgen deprivation therapy was leuprolide, except for 1 patient who chose orchiectomy. Five of the patients had testosterone levels measured within 1 year before developing castration resistance, and the remaining 2 patients did not have any serum testosterone levels recorded in their medical records. The 5 patients with serum testosterone data had the following levels immediately before or on the day they were determined to have castration resistance: 3.7, 9, <12, 19, and 58 ng/mL. The patient with the testosterone level of 58 ng/mL as well as the 2 patients without measured testosterone levels were determined to have clinical evidence of castration resistance because of a continual rise in PSA despite adding a second agent to their androgen deprivation therapy.

Univariate analysis using Cox regression of typical prognostic variables versus FFBF revealed that only the highest Gleason score ($P=.0290$) was statistically significant (Table 3). The EZH2 grade ($P=.07$) trended toward significance. Although tumor DAB2IP status was nearly significant by Cox regression ($P=.055$), as stated earlier the log-rank test for DAB2IP versus FFBF was significant ($P=.04$). Further analysis showed that reduction of DAB2IP is strongly correlated with increasing Gleason score (Fig. 2; $P=.0087$), suggesting that DAB2IP reduction leads to more aggressive phenotypes of prostate cancer.

Discussion

Disabled homolog 2-interacting protein, a tumor suppressor and member of the RAS-GAP family, has been linked with an increased risk of aggressive cancer (12). Although the exact function of DAB2IP has yet to be determined, studies have shown that loss of DAB2IP leads to hyper-activation of the PI3K-AKT axis (16). Disabled homolog 2-interacting protein–deficient cell lines are more resistant to ionizing radiation owing an increased ability to repair double-strand DNA breaks and promote robust G2/M cell cycle arrest (14, 21). Furthermore, cells that lack DAB2IP

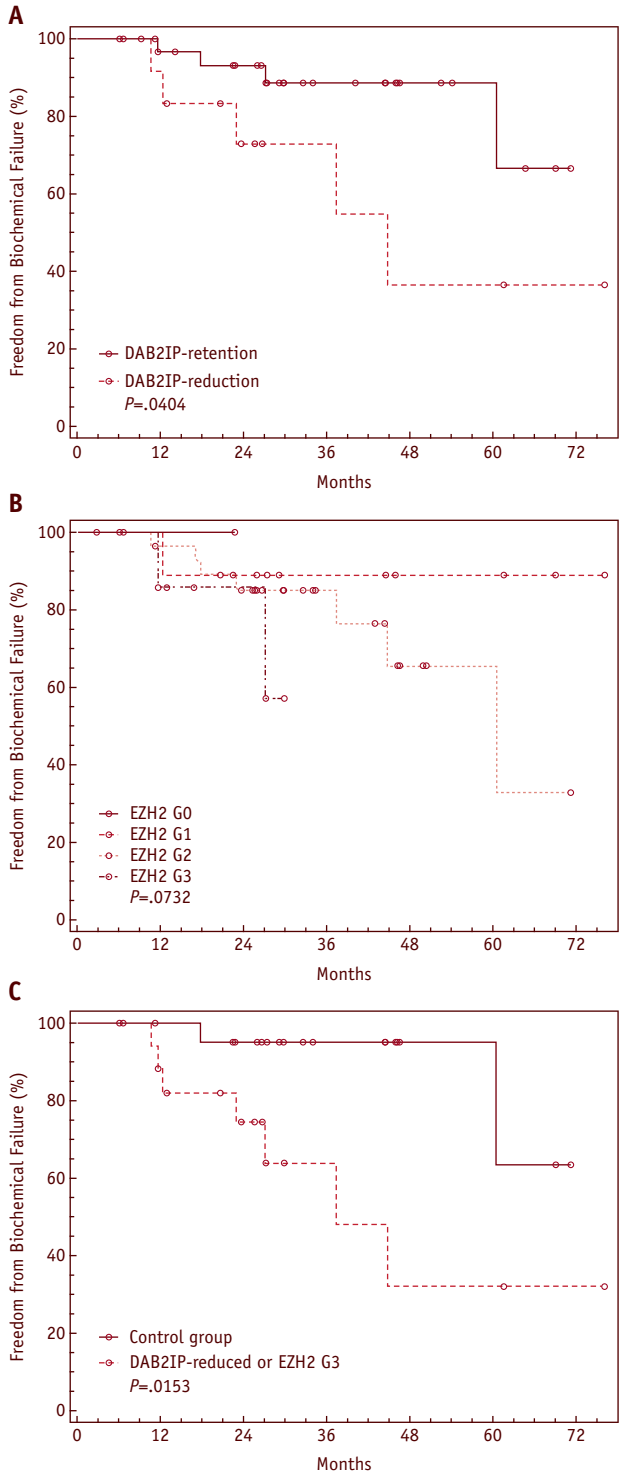

Fig. 1. Kaplan-Meier and log-rank analysis comparing freedom from biochemical failure in patients according to (A) protein DAB2IP tumor status, (B) stratified enhancer of zeste homolog 2 (EZH2) tumor status, and (C) reduced DAB2IP or grade 3 EZH2 expression compared with the control group of patients with both retained DAB2IP and grade 0-2 EZH2 expression.

are more likely to undergo autophagy, rather than apoptosis, in response to ionizing radiation (15). On the basis of strong preclinical data indicating the role of DAB2IP in radiation response in prostate cancer cells, we sought to determine its clinical impact (15). However, the tumor environment is a complex milieu with multiple interacting activators and inhibitors. Therefore, in addition to studying DAB2IP, we also sought to determine the potential prognostic role of its upstream regulator, EZH2, in high-risk prostate cancer patients treated with radiation therapy.

In this pilot study we show that DAB2IP status and not EZH2 seems to correlate with earlier biochemical failure rates after treatment with definitive radiation therapy in high-risk prostate cancer patients. Interestingly, we found that nearly all high-risk prostate cancer samples in this study express high levels of EZH2, confirming the notion that increased EZH2 precedes loss of DAB2IP. Our results are concordant with previous studies that show increased levels of EZH2 portend a poorer outcome, or more specifically, increased EZH2 levels can predict high-risk prostate cancer. It is worth emphasizing that the trend toward worse outcomes occurred despite patients with higher EZH2 levels having been significantly more likely to receive hormone therapy ($P = .0417$). Varambally et al (20) noted that EZH2 G3 staining or greater was associated with increased clinical failure (31%), whereas significantly fewer patients (9%) with low-intensity staining had clinical failure. Although the patients evaluated in Varambally's study received surgical management and not radiation, the results support the conclusions presented here.

Rather than predict cancers with poor therapeutic response, EZH2 levels may help screen for higher-risk cancers. In addition, it is possible that if the cohort were expanded to include all prostate cancer patients (including low- and intermediate-risk patients), then EZH2 will likely gain significance, and it may serve as an earlier marker of tumors that may have propensity toward high-risk differentiation. However, within the high-risk cohort of patients, DAB2IP seems to be a more suitable prognostic marker because it seems to be able to discriminate out the very worst players among this locally advanced aggressive prostate cancer group. We postulate that the higher the intensity of EZH2 staining, the more likely a tumor is to have decreased DAB2IP expression, and thus the more likely a patient is to have poor outcome. This theory is the logic behind using the "or" in our combined grouping system: that perhaps tumors with EZH2 G3 and retained DAB2IP will eventually manifest future DAB2IP loss and consequently become more aggressive.

There have been numerous studies into the use of biomarkers in prostate cancer, and although most are used for the evaluation of surgical patients, several studies have studied markers of radiation outcomes. The most successful studies have examined markers such as Ki-67, Bax, BCL-2, and BCL-xL, which are markers of apoptosis (8, 9). However, results from these studies are heterogeneous and conflicting. DAB2IP protein may be better able to

Table 2 Patient outcomes by tumor biomarker status

Biomarker status	FFBF		CRFS		DMFS	
	4 y (%)	*P*	4 y (%)	*P*	4 y (%)	*P*
DAB2IP-retained	88.70	.0404	89.90	.0172	96.60	.0526
DAB2IP-reduced	36.50		50.00		36.00	
EZH2 G0	100.00	.0732	100.00	.0722	100.00	.2035
EZH2 G1	88.90		83.30		88.90	
EZH2 G2	65.50		81.50		100.00	
EZH2 G3	57.10		0.00		83.30	
DAB2IP-reduced or EZH2 G3	31.90	.0153	27.90	.0019	39.40	.0401
Control group	95.00		100.00		100.00	

Abbreviations: CRFS = castration resistance–free survival; DMFS = distant metastasis–free survival; FFBF = freedom from biochemical failure; G = grade. Other abbreviations as in Table 1.
The top 2 rows compare patient outcomes according to retained versus reduced levels of DAB2IP. The middle 4 rows compare patient outcomes according to the stratified intensity level of EZH2 expression. The bottom 4 rows compare patient outcomes with reduced DAB2IP or grade 3 EZH2 expression, versus the control group of patients with both retained DAB2IP and grade 0-2 EZH2 expression.

differentiate the worst cases among the already high-risk group of prostate cancer patients. In this pilot study, DAB2IP seems to be a significant prognostic indicator of failure after radiation therapy; however, DAB2IP requires further studies to validate its role in this cohort of patients and to further determine whether it may also be a predictive marker of response to radiation therapy. Limitations of this study include the small sample size, short follow-up for patients with EZH2 G0 and G3, and the fact that not all 54 patients had adequate biopsy samples to be analyzed for both DAB2IP and EZH2. With increased sample size and longer follow-up, it is possible that stratified EZH2 expression may also be a useful and statistically significant prognostic biomarker. Because this is a pilot study, a prospective validation study with a larger sample size is warranted.

Table 3 Univariate Analysis

Variable	HR (95% CI)	*P*-value
DAB2IP Status (Reduced vs. Retained)	3.7 (1.0-13.7)	.055
EZH2 Grade (Continuous)	2.9 (0.9-9.3)	.073
T-Stage (Continuous)	1.1 (0.7-1.6)	.746
N-Stage (N0 vs. N1)	2.9 (0.6-14.1)	.182
Gleason Score (Continuous)	2.1 (1.1-4.2)	.029
PSA Pretreatment (Continuous)	1.0 (1.0-1.0)	.970
% Core Positivity (Continuous)	3.7 (0.3-42.6)	.299
Total Radiation Dose (Continuous)	0.9 (0.7-1.3)	.703
Hormone Therapy (No vs. Yes)	3.5 (0.4-31.5)	.261
Duration of Hormone Therapy (Continuous)	1.0 (0.9-1.1)	.512

Abbreviations: CI = confidence interval; HR = hazard ratio. Other abbreviations as in Table 1.
By log-rank test DAB2IP ($P = .040$) was significant. By Cox regression, Gleason score ($P = .029$) was statistically significant, whereas DAB2IP ($P = .055$) and EZH2 ($P = .073$) trended toward significance.

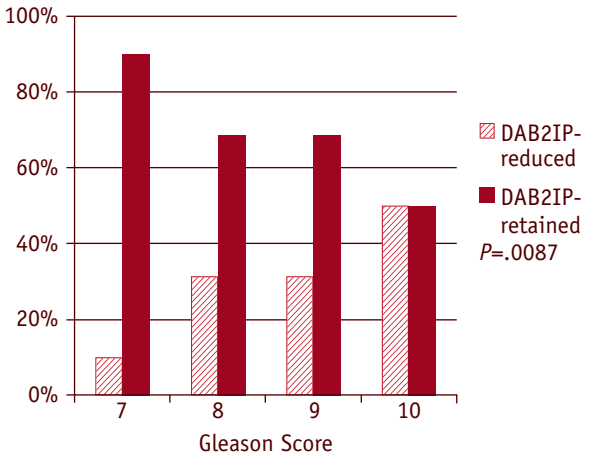

Fig. 2. Decreased DAB2IP protein expression within prostatic adenocarcinoma correlates with a higher Gleason score.

We report that loss of DAB2IP may predict worse FFBF and increased likelihood of progression to castration resistance. Decreased FFBF in DAB2IP-deficient cells may be explained by dysregulation of survival pathways in response to ionizing radiation as described in several preclinical models. In addition, high Gleason scores correlate with a loss of DAB2IP. These findings may indicate that loss of DAB2IP may be a driver of prostate cancer progression, or alternatively that DAB2IP loss may be a hallmark for aggressive prostate cancer behavior. A recently published study determined that androgen binding decreases EZH2 level with a concomitant increase in DAB2IP level (24), which is consistent with our previous observation that DAB2IP is a target gene of EZH2 in prostate cancer (18). Another study found that DAB2IP expression was inversely related to androgen receptor activation in an androgen-independent manner (25). The potential relation of DAB2IP to castration resistance may suggest an interaction of DAB2IP or its downstream proteins with the androgen receptor or interactions with androgen receptor elements.

As a prognostic biomarker, DAB2IP may identify patients at highest risk for treatment failure before initiation of standard therapy. Potential clinical application is that in the future we may be able to effectively use DAB2IP presence or absence from a patient's biopsy specimen as a means of determining curability of their cancer with standard radiation-based therapeutic regimens. Additionally, the DAB2IP pathway may be a potential target for improving treatment outcome and radiation response. Future research may be directed toward creating molecularly based therapeutic strategies to up-regulate DAB2IP and restore the tumor suppressor's presence within the neoplastic cells, or by targeting downstream effectors such as clusterin (26).

This pilot study gives us a rationale to consider further validation study of DAB2IP and EZH2. Disabled homolog

2-interacting protein status in combination with highest EZH2 expression (G3) may be useful for determining patients with worse outcome within the high-risk prostate cancer population.

References

1. Siegel R, Naishadham D, Jemal A. Cancer statistics, 2013. *CA Cancer J Clin* 2013;63:11-30.
2. Punnen S, Cooperberg MR. The epidemiology of high-risk prostate cancer. *Curr Opin Urol* 2013;23:331-336.
3. Mohler JL. The 2010 NCCN clinical practice guidelines in oncology on prostate cancer. *J Natl Compr Canc Netw* 2010;8:145.
4. Horwitz EM, Bae K, Hanks GE, et al. Ten-year follow-up of radiation therapy oncology group protocol 92-02: A phase III trial of the duration of elective androgen deprivation in locally advanced prostate cancer. *J Clin Oncol* 2008;26:2497-2504.
5. Bolla M, de Reijke TM, Van Tienhoven G, et al. Duration of androgen suppression in the treatment of prostate cancer. *N Engl J Med* 2009; 360:2516-2527.
6. Bolla M, Van Tienhoven G, Warde P, et al. External irradiation with or without long-term androgen suppression for prostate cancer with high metastatic risk: 10-year results of an EORTC randomised study. *Lancet Oncol* 2010;11:1066-1073.
7. Hanks GE, Pajak TF, Porter A, et al. Phase III trial of long-term adjuvant androgen deprivation after neoadjuvant hormonal cytoreduction and radiotherapy in locally advanced carcinoma of the prostate: The Radiation Therapy Oncology Group Protocol 92-02. *J Clin Oncol* 2003;21:3972-3978.
8. Pollack A, Cowen D, Troncoso P, et al. Molecular markers of outcome after radiotherapy in patients with prostate carcinoma: Ki-67, bcl-2, bax, and bcl-x. *Cancer* 2003;97:1630-1638.
9. Mackey TJ, Borkowski A, Amin P, et al. bcl-2/bax ratio as a predictive marker for therapeutic response to radiotherapy in patients with prostate cancer. *Urology* 1998;52:1085-1090.
10. Bibault JE, Fumagalli I, Ferte C, et al. Personalized radiation therapy and biomarker-driven treatment strategies: A systematic review. *Cancer Metastasis Rev* 2013;32:479-492.
11. Chen H, Toyooka S, Gazdar AF, et al. Epigenetic regulation of a novel tumor suppressor gene (hDAB2IP) in prostate cancer cell lines. *J Biol Chem* 2003;278:3121-3130.
12. Duggan D, Zheng SL, Knowlton M, et al. Two genome-wide association studies of aggressive prostate cancer implicate putative prostate tumor suppressor gene DAB2IP. *J Natl Cancer Inst* 2007;99:1836-1844.
13. Min J, Zaslavsky A, Fedele G, et al. An oncogene-tumor suppressor cascade drives metastatic prostate cancer by coordinately activating Ras and nuclear factor-[kappa]B. *Nat Med* 2010;16:286-294.
14. Kong Z, Xie D, Boike T, et al. Downregulation of human DAB2IP gene expression in prostate cancer cells results in resistance to ionizing radiation. *Cancer Res* 2010;70:2829-2839.
15. Yu L, Tumati V, Tseng SF, et al. DAB2IP regulates autophagy in prostate cancer in response to combined treatment of radiation and a DNA-PKcs inhibitor. *Neoplasia* 2012;14:1203-1212.
16. Xie D, Gore C, Zhou J, et al. DAB2IP coordinates both PI3K-Akt and ASK1 pathways for cell survival and apoptosis. *Proc Natl Acad Sci U S A* 2009;106:19878-19883.
17. Bachmann IM, Halvorsen OJ, Collett K, et al. EZH2 expression is associated with high proliferation rate and aggressive tumor subgroups in cutaneous melanoma and cancers of the endometrium, prostate, and breast. *J Clin Oncol* 2006;24:268-273.
18. Chen H, Tu SW, Hsieh JT. Down-regulation of human DAB2IP gene expression mediated by polycomb Ezh2 complex and histone deacetylase in prostate cancer. *J Biol Chem* 2005;280:22437-22444.
19. Rhodes DR, Sanda MG, Otte AP, et al. Multiplex biomarker approach for determining risk of prostate-specific antigen-defined recurrence of prostate cancer. *J Natl Cancer Inst* 2003;95:661-668.
20. Varambally S, Dhanasekaran SM, Zhou M, et al. The polycomb group protein EZH2 is involved in progression of prostate cancer. *Nature* 2002;419:624-629.
21. Kong Z, Raghavan P, Xie D, et al. Epothilone B confers radiation dose enhancement in DAB2IP gene knock-down radioresistant prostate cancer cells. *Int J Radiat Oncol Biol Phys* 2010;78:1210-1218.
22. Wang Z, Tseng CP, Pong RC, et al. The mechanism of growth-inhibitory effect of DOC-2/DAB2 in prostate cancer: Characterization of a novel GTPase-activating protein associated with N-terminal domain of DOC-2/DAB2. *J Biol Chem* 2002;277:12622-12631.
23. Roach M, Hanks G, Thames H, et al. Defining biochemical failure following radiotherapy with or without hormonal therapy in men with clinically localized prostate cancer: Recommendations of the RTOG-ASTRO Phoenix Consensus Conference. *Int J Radiat Oncol Biol Phys* 2006;65:965-974.
24. Bohrer LR, Chen S, Hallstrom TC, et al. Androgens suppress EZH2 expression via retinoblastoma (RB) and p130-dependent pathways: A potential mechanism of androgen-refractory progression of prostate cancer. *Endocrinology* 2010;151:5136-5145.
25. Wu K, Liu J, Tseng SF, et al. The role of DAB2IP in androgen receptor activation during prostate cancer progression. *Oncogene* 2014; 33:1954-1963.
26. Wu K, Xie D, Zou Y, et al. The mechanism of DAB2IP in chemoresistance of prostate cancer cells. *Clin Cancer Res* 2013;19:4740-4749.

Journal of Biomedical Materials Research Part A

POLYMERIC NANOPARTICLES FOR TARGETED RADIOSENSITIZATION OF PROSTATE CANCER CELLS

Journal:	*Journal of Biomedical Materials Research: Part A*
Manuscript ID:	JBMR-A-14-0455.R1
Wiley - Manuscript type:	Original Article
Date Submitted by the Author:	n/a
Complete List of Authors:	Menon, Jyothi; The University of Texas Southwestern Medical Center, Graduate Program in Biomedical Engineering; The University of Texas at Arlington, Department of Bioengineering Tumati, Vasu; The University of Texas Southwestern Medical Center, Department of Radiation Oncology Hsieh, Jer-Tsong; The University of Texas Southwestern Medical Center, Department of Urology; The University of Texas Southwestern Medical Center, Simmons Comprehensive Cancer Center Nguyen, Kytai; The University of Texas Southwestern Medical Center, Graduate Program in Biomedical Engineering; The University of Texas at Arlington, Department of Bioengineering Saha, Debabrata; The University of Texas Southwestern Medical Center, Department of Radiation Oncology
Keywords:	Nanoparticles, Radiosensitization, Prostate cancer, NU7441, Targeting

POLYMERIC NANOPARTICLES FOR TARGETED RADIOSENSITIZATION OF PROSTATE CANCER CELLS

Jyothi U. Menon[1,2], Vasu Tumati[3], Jer-Tsong Hsieh[4, 5], Kytai T. Nguyen[1,2], Debabrata Saha[3,5*]

[1]Department of Bioengineering, The University of Texas at Arlington, Arlington, TX, 76019

[2]Graduate Program in Biomedical Engineering, The University of Texas Southwestern Medical Center, Dallas, TX, 76019

[3] Department of Radiation Oncology, [4] Department of Urology, [5]Simmons Comprehensive Cancer Center, The University of Texas Southwestern Medical Center, Dallas, TX, 75390

Running Title: Nanoparticles for radiosensitization of prostate cancer cells

***Corresponding Author:**

Debabrata Saha, Ph.D.
Department of Radiation Oncology
Division of Molecular Radiation Biology
The University of Texas Southwestern Medical Center
2201 Inwood Road, Dallas, TX 75390-9187; USA
Email: debabrata.saha@utsouthwestern.edu
Tel: (214) 648-7750
FAX: (214) 648-5995

ABSTRACT

One of the many issues of using radiosensitizers in a clinical setting is timing daily radiation treatments to coincide with peak drug concentration in target tissue. To overcome this deficit, we have synthesized a novel nanoparticle system consisting of poly (lactic-co-glycolic acid) (PLGA) nanoparticles conjugated with prostate cancer cell penetrating peptide-R11 and encapsulated with a potent radio-sensitizer 8-dibenzothiophen-4-yl-2-morpholin-4-yl-chromen-4-one (NU7441) to allow prostate cancer-specific targeting and sustained delivery over 3 weeks. Preliminary characterization studies showed that the R11-conjugated nanoparticles (R11-NU7441 NPs) had an average size of about 274 $\pm$ 80 nm and were stable for up to 5 days in de-ionized water and serum. The nanoparticles were cytocompatible with immortalized prostate cells (PZ-HPV-7). Further, the particles showed a bi-phasic release of encapsulated NU7441 and were taken up by PC3 prostate cancer cells in a dose- and magnetic field-dependent manner while not being taken up in non-prostate cancer cell lines. In addition, R11-NU7441 NPs were effective radiation sensitizers of prostate cancer cell lines *in vitro*. These results thus demonstrate the potential of R11-conjugated PLGA NPs as novel platforms for targeted radiosensitization of prostate cancer cells.

Keywords : Nanoparticles, radiosensitization, prostate cancer, NU7441, targeting

1. INTRODUCTION

Prostate cancer remains one of the leading causes of cancer-related mortality in men with an estimated 233,000 new cases and 29,480 deaths expected by the end of 2014.[1] Conventional treatment methods for this disease include surgery or radiation therapy. Ionizing radiation therapy is an established method of treatment of localized prostate cancer; however, many high-grade tumors display radiation resistance and often recur after therapy. High-grade prostate cancers are often radiation resistant because of their increased DNA double strand break (DSB) repair ability, especially through Non-Homologous End Joining (NHEJ) [2]. Previously, studies have shown that 8-dibenzothiophen-4-yl-2-morpholin-4-yl-chromen-4-one (NU7441) is a highly potent compound that can selectively inhibit DNA-dependent protein kinase (DNA-PKcs), a central regulator of NHEJ. As a result of DNA-PKcs inhibition, cells are unable to effectively repair DNA damage and die through various mechanisms.[3] Although NU7441 has demonstrated excellent radiosensitization both *in vitro* and *in vivo*, this compound is limited by its poor solubility in water and reduced oral bioavailability.[4] Therefore there is an urgent need for alternative methods that facilitate localized NU7441 delivery for effective radiosensitization.

In recent years there has been a push for localized therapy in hopes of reducing normal tissue effects as well as limiting side effects of the treatment. Nanoparticles (NPs) have become central players in the localized therapy push. NPs have been used successfully as radiation sensitizers; specifically, several studies have shown that gold can radiosensitize prostate cancer cells by arresting the cell cycle into G2/M. [5] Similarly, Jin et al.[6] have synthesized poly lactic-co-glycolic acid (PLGA) NPs encapsulating etanidazole (SR-2508), which successfully radiosensitized hypoxic HeLa cervical cancer and MCF-7 breast cancer cells. However, multifunctional NPs capable of delivering the radiosensitizer, imaging and cancer targeting of

the prostate cancer cells have not been studied so far. Also, there have been no studies to the authors' knowledge on the development of NU7441-incorporated NPs for the potent radiosensitization of prostate cancers.

Therefore in this study, multifunctional PLGA-based NPs were synthesized for sustained release of NU7441 for targeted radiosensitization of prostate cancer cells. The FDA-approved biocompatible and biodegradable PLGA is a commonly used polymer in drug delivery and is known to provide a sustained release of the encapsulated agent over time both by degradation and diffusion.[7] Iron oxide NPs were incorporated as contrast agents for Magnetic Resonance Imaging (MRI), for magnetic targeting and also to induce hyperthermia in the tumor using an external alternating magnetic field.[8,9] To increase the target specificity of PLGA particles, the particles were further conjugated with R11-a polyarginine cell permeable peptide with prostate specificity,[10] to form R11-NU7441 NPs. Studies conducted previously have already shown that the R11 peptides have higher specificity and uptake efficiency by prostate cancer cells in comparison with other cell-penetrating peptides such as TAT, KALA, penetratin and L-lysine K11.[11] Further, we have also previously demonstrated the significantly higher accumulation of R11-conjugated thermoresponsive NPs in the prostate tumor of NOD SCID mice, compared to other vital organs.[12] In this study, R11-conjugated PLGA-based NPs containing NU7441 were synthesized to selectively enhance the radiation sensitivity of prostate cancer cells.

2. MATERIALS AND METHODS

2.1. Preparation of R11-conjugated, NU7441-loaded NPs

The PLGA magnetic NPs (PLGA-MNPs) were prepared using a single emulsion technique in which PLGA (Lakeshore Biomaterials, Birmingham, AL), bare iron oxide NPs

(Meliorum technologies, Rochester, NY), and NU7441 (Tocris Biosciences, Minneapolis, MN) solution in dichloromethane (DCM) formed the organic/ oil phase. This mixture was then sonicated and added dropwise to 5% (w/v) poly vinyl alcohol (PVA) solution which was the aqueous/ water phase. The resultant solution was further sonicated at 50W for 3 minutes using a high-speed sonicator following which it was allowed to stir overnight to allow evaporation of DCM. This sample was then centrifuged and the pellet containing the NPs was freeze-dried. The supernatant obtained after centrifugation was saved to determine the amount of unloaded drug, against an NU7441 standard curve. This amount was subtracted from the original amount of drug used, to determine the total drug amount loaded in the NPs.

For preparation of R11-NU7441 NPs, 5 mg of the freeze-dried unconjugated NPs were taken and dissolved in 2-(*N*-morpholino)ethanesulfonic acid (MES) buffer (pH ~4.7). Then 1-Ethyl-3-(3-dimethylaminopropyl) carbodiimide (EDC) and N-hydroxy succinimide (NHS) was added with 30 minutes incubation following addition of each chemical. Lastly, 380 µg of R11 peptide was added and the solution was kept for shaking at room temperature overnight. The sample was washed and freeze-dried to obtain R11-conjugated NPs.

2.2. Characterization studies

Dynamic light scattering (DLS) (ZetaPals Analyzer, Brookhaven Instruments, Holtsville, NY) was used to study the size, surface charge and zeta potential of unconjugated and R11-NU7441 NPs. Briefly, the NP suspension was added to transparent cuvettes and inserted into the machine where scattering of laser light by the Brownian motion of NPs gave values for physical characterization of the particles. Additionally, a drop of NP suspension was added to a 200-mesh Formvar-coated copper grid (Electron Microscopy Sciences, Hatfield, PA) and air-dried for

observation of NP morphology using Transmission Electron Microscopy (TEM, FEI Tecnai G2 Spirit BioTWIN, Hillsboro, OR). Further, Fourier Transform Infrared spectroscopy (FTIR, Bruker VECTOR 22 spectrometer, Madison, WI) was used to determine the successful conjugation of R11 and incorporation of iron oxide within the PLGA NPs. Iron content was determined based on a standard iron assay as described previously.[13] Briefly, the NP solution was incubated with 30% (v/v) hydrochloric acid at 55°C for 2 h. Then ammonium persulfate (APS, 1mg/ml) and potassium thiocyanate (0.1 M) was added consecutively to the solution followed by 15 mins shaking. The iron concentration in the NPs was determined by obtaining absorbance readings at 520 nm, which was compared against iron oxide NP standards. A superconducting quantum interference device (SQUID, Quantum design, CA) magnetometer was also used to study the superparamagnetic behavior of iron oxide-encapsulated NPs. Briefly, the NPs were embedded in an epoxy gel and mounted on the instrument using a plastic straw. The behavior of the NPs in response to changing magnetic field at room temperature was determined.

Following initial characterization, the NPs were further studied for their stability and drug release kinetics. The NPs were suspended in de-ionized (DI) water and 10% Fetal bovine serum (FBS) in RPMI 1640 media for a period of 5 days at 37°C and particle size was measured at every 24 hour-time point using DLS. To study the drug release kinetics, 1 mg/ml NP suspension was added to 1000 Da Molecular weight cut-off (MWCO) dialysis bags (Spectrum laboratories, Rancho Dominguez, CA) and shaken at 37°C for 21 days. At pre-determined time points, 1 ml of the dialysate was removed and 1 ml of fresh DI water was added. The removed dialysate was stored at -20°C for further analysis. The amount of NU7441 released was analyzed against NU7441 standards (0.5, 0.25, 0.0125, 0.0625, 0.03125, 0.0156, 0 mg/ml) at an excitation/emission wavelength of 470/585 nm using a UV spectrofluorometer.

2.3. *In vitro* toxicity study

To study the toxicity of our NPs, a 96-well plate was first seeded with immortalized human prostate epithelial cells, PZ-HPV-7 at a seeding density of 15,625 cells/cm^2 and incubated at 37^{o}C overnight. Cells were incubated with increasing concentration of R11-NU7441 NPs (0, 250, 500, 1000, 2000 µg/ml) and incubated at 37^{o}C for 24 hours. The cells were washed thrice with 1X PBS and cell viability was assessed using MTS Assays (Promega Corporation, Madison, WI) per the manufacturer's directions. Briefly, 200 µl of media and 20 µl of MTS reagent were added to each well and the wellplate was incubated in the dark at 37^{o}C for about 2 hours. Media in wells containing greater number of cells would be more purplish in color due to the bioreduction of the tetrazolium compound in MTS reagent into purple formazan crystals by the cells. Absorbance values of each sample was obtained at 490 nm using a spectrometer.

2.4. Rate of cellular uptake of NPs

The dose- and magnetic field-dependent uptake of unconjugated NPs and R11-NU7441 NPs by PC3 prostate cancer cells was assessed in the presence and absence of a 1.3 Tesla (T) magnet. The cells were seeded at a density of 12,631 cells/cm^2 in a 48-well plate and allowed to grow for 24 hours. The PC3 cells were seeded at lower seeding density to ensure that these rapidly dividing cells do not become overconfluent and die due to insufficient growth area, for the duration of the experiment. A 96 wellplate was used for cytotoxicity study above as only one assay (MTS assay) was required to be conducted for this study. For cellular uptake study, a greater volume of cell lysis samples was required as 2 assays (iron assay and BCA protein assay) were to be conducted to determine the amount of NPs and the amount of cell/ total protein per

well. Therefore the 48 wellplate was used so that sufficient sample would be available for analysis. Following 24 hour incubation, the PC3 cells were exposed to increasing concentration of NP suspension (0, 100, 200, 300, 500, 1000 μg/ml) in media and incubated for 2 hours. To study magnetic field-dependence of uptake, the well-plate was placed directly above a 1.3 T external magnet to ensure that the cells are uniformly exposed to the magnetic field. These cells were then incubated at 37°C for 2 hours. The following day, the media was aspirated and the cells were washed with phosphate buffered saline (PBS) before being lysed using 1% Triton X-100. The iron oxide present within the cells was quantified using iron assay as explained previously.[13] A Pierce BCA protein assay was also performed to determine the amount of cell protein per well for normalization of iron oxide taken up by the cells.

2.5. Colony Formation Assay

Exponentially growing prostate and lung cancer cells were treated with either control or R11-NU7441 NPs for 4 hours in the absence of a magnet. After incubation, cells were washed and then treated with increasing doses of ionizing radiation (IR) (0, 2, 4, 6, and 8 Gy). Cells were then trypsinized and counted using a particle counter (Beckman Coulter, Inc., Brea, CA), diluted serially to appropriate concentrations and plated into 60-mm dish in triplicate. After 7 to 14 days of incubation, the colonies were fixed and stained with 4% formaldehyde in PBS containing 0.05% crystal violet. Colonies containing >50 cells were counted. Surviving fraction was calculated as (mean colony counts)/[(cells plated) × (plating efficiency)], in which plating efficiency was defined as (mean colony counts)/(cells plated for unirradiated controls). The data are presented as the mean ± SD of at least three independent experiments. The curve $S = e^{-(\alpha D + \beta D2)}$ was fitted to the experimental data using a least square fit algorithm and the program Sigma

Plot (Systat Software, Inc., San Jose, CA). The radiation dose enhancement ratio (DER) was calculated as the dose (Gy) for radiation alone divided by the dose (Gy) for radiation plus drugs (normalized for drug toxicity) for a surviving fraction of 0.25.

2.6. DNA Double Strand Break Repair Assay

DSB repair assay was performed by counting phospho-γH2AX foci after IR, NP and IR+NP treatment. These cells were plated on poly-lysine-coated coverslips, were allowed to attach overnight and then treated with either control or R11 conjugated NU7441 NPs for 4 hours in the absence of a magnet, followed by washing with PBS and irradiated at 2 Gy. Cells were fixed in 4% formaldehyde/PBS for 30 minutes, permeabilized in 0.5% Triton X-100 in PBS for 1 hour, and blocked in 5% bovine serum albumin and 1% normal goat serum for 1 hour at room temperature. Then, cells were incubated with the primary antibody, anti–phospho-Histone γH2AX (Ser139; 1:2,000) for 1 hour. Rhodamine red–conjugated goat anti-mouse was used as secondary antibodies. Cells were mounted in a Vectashield mounting medium containing 4′, 6-diamidino-2-phenylindole (DAPI). Phospho-γH2AX foci were examined using a fluorescence microscope (CRG Precision Electronics, Houston, TX). The number of phospho-γH2AX foci was determined at each time point (average of 100 nuclei), and the percentage foci remaining was plotted against time to obtain DSB repair kinetics. Data is represented as mean ± SEM.

3. RESULTS

3.1. Characterization of R11-NU7441 NPs

An average diameter of 265.5± 64.0 and 274.13± 79.96 nm was observed for the unconjugated NPs and R11-conjugated NU7441 NPs respectively. The polydispersity values in

the range of 0.12-0.l6 indicated that the particles are uniformly dispersed with minimal size variation. Additionally, high zeta potential values of -17.39 $\pm$ 0.58 and -24.52 $\pm$ 0.54 indicated that both the conjugated and non-conjugated NPs are very stable and do not aggregate. The TEM images concurred with DLS results and indicate that our NPs are spherical in shape with iron oxide presented in the particles (Fig. 1A). Iron assay results indicated the presence of 8.44% iron content within our R11-NU7441 NPs, which could be attracted towards an external magnet (1.3T) (Fig. 1B).

The NPs were further characterized for the presence of functional groups that can confirm peptide conjugation and inclusion of iron oxide, using Fourier Transform Infrared spectroscopy (FTIR). The peak at ~ 590 cm^{-1} confirms presence of Fe-O group. The NH_2 peak at 1420 cm^{-1} and NH peak at 1500 cm^{-1} is characteristic of Arginine present in R11 peptide indicating successful R11-conjugation. The CH_2 (2850 cm^{-1}) and C=O peaks (1740 cm^{-1}) are characteristic of PLGA. The C=O peak can also represent O=C-N-H bond formed during EDC-NHS chemistry for R11 conjugation (Fig. 1C). Further, analysis of SQUID measurements indicated that our particles maintained their superparamagnetic behavior although a decrease in saturation magnetization to 48.64 emu/g was observed (Fig. 1D). A remanence and coercivity of 6.21 (Mr/Ms) and 85.009 Oe respectively was observed for the NPs in comparison to 6.7 (Mr/Ms) remanence and 75.556 Oe coercivity of bare iron oxide NPs.

Results from the stability studies showed that there was no statistically significant change in particle size of the R11-NU7441 NPs in DI water and 10% FBS over a period of 5 days (Fig. 2). This indicates that our particles are relatively stable and are not expected to aggregate under physiological conditions.

3.2. Drug loading and release kinetics

The release of NU7441 from our NPs was monitored over a period of 21 days. The particles showed a loading efficiency of 51.89% for NU7441. A burst release of about 41% of the encapsulated drug was observed within 1 day of the study, followed by sustained release of 90.48% of the encapsulated NU7441 from the NPs within 3 weeks (Fig. 3).

3.3. *In vitro* cell studies on R11-NU7441 NPs

Cytocompatibility studies showed greater than 80% PZ-HPV-7 viability up to an NP concentration of 1000 µg/ml (Fig. 4A). Viability at 2000 µg/ml concentration was significantly less than the control group, although ~80% of the cells were still viable. This demonstrates that our R11-NU7441 NPs are cytocompatible with no toxic effects observed even at a high concentration of 1000 µg/ml.

Further, cellular uptake of unconjugated NPs by PC3 cells in the presence of a magnet was found to be significantly lower than uptake of R11-NU7441 NPs both in the presence and absence of a magnet. All particles were taken up by PC3 cells in a dose-dependent manner; however, the highest uptake was observed for R11-conjugated NPs in the presence of an external magnetic field (1.3T) (Fig. 4B). This indicates that although R11 conjugation significantly improves NP uptake by PC3 cells, an external magnetic field can facilitate greater cellular uptake of the R11-NU7441 NPs.

3.4. DNA DSB Repair Kinetics

To test both the efficacy and specificity of R11-NU7441 NPs, both lung and prostate cancers were treated with NPs to determine the specificity of R11 targeting and the efficacy of

NU7441 release. In H460, a non-small cell lung cancer cell line, treatment with R11 conjugated NPs and radiation did not result in decreased DNA DSB repair kinetics (Fig. 5A). However, in PC3, a prostate cancer cell line, treatment with R11 conjugated NPs and radiation resulted in significantly slower DNA repair kinetics (Fig. 5B). The results of this experiment imply that R11-NU7441 NPs will specifically target prostate cancer cells and also radiosensitize these cells.

3.5. Colony Formation Assay

To further explore the radiosensitizing ability of R11-NU7441 NPs, lung and prostate cancer cells were treated with radiation and a dummy particle containing no NU7441 or radiation and R11-NU7441 NPs. As with the DNA DSB break repair assay H460 cells show no radiation sensitization (Fig. 6A), while PC3 cells show a prominent radiation sensitizing effect (Fig. 6B).

4. DISCUSSION

Recent years have shown a growing interest and demand for multifunctional "theranostic" NPs capable of simultaneous diagnosis and treatment of the disease of interest. In this study, we have synthesized novel multifunctional R11-conjugated PLGA NPs encapsulating MNPs and NU7441 for targeted delivery, imaging and radiation sensitization of prostate cancer cells. PLGA NPs encapsulating various payloads have often been used for numerous cancer-based applications. For example, curcumin-loaded PLGA NPs (81 nm) have been successfully used to inhibit cellular proliferation in DU145 prostate cancer cells *in vitro* and have shown greater bioavailability than free curcumin when administered *in vivo*.[14] Lipid-coated PLGA NPs (~ 207 nm) containing KIF11 small interfering RNA (siRNA) could successfully reduce cell viability of PC3, LNCaP and DU145 prostate cancer cells *in vitro*.[15] Also as mentioned earlier,

PLGA NPs have played key roles in radiation sensitization of cervical and breast cancer cells using a combination of drugs.[6,16]

Although the average diameter of our R11-NU7441 NPs is >200 nm, particles in this size range have been used previously by other groups for cancer therapy. For example, Alendronate-coated PLGA-iron oxide NPs (235 nm) were synthesized by Thamake et al. [17] for specific targeting of bone metastasis of breast cancer. *In vivo* studies on athymic female nude mice demonstrated that these particles showed high localization to the bone and could significantly reduce tumor-induced bone resorption as well as tumor growth rate. Our lab has also previously synthesized core-shell NPs of 296 nm diameter for melanoma targeted therapy. These particles showed significantly higher localization than unconjugated NPs, in the tumor of B16F10 melanoma orthotopic mouse model indicating that they can be used for targeted melanoma therapy.[18] Our particles also maintained the superparamagnetic behavior of iron oxide, although a slight decrease in saturation magnetization (48.64 emu/g) is noted in R11-NU7441 NPs. This result is expected due to the presence of the polymer which tends to generate a diamagnetic moment in response to the applied magnetic field.[18,19] However, NPs having similar or lower magnetization values have been used previously for various drug delivery applications with some degree of success, [20,21] indicating that our particles remain within the range suitable for targeted drug delivery. Our stability study results concur with previous studies on PLGA NPs showing good stability and minimal aggregation over a period of 5 days.[22] Also, the drug release kinetics of our particles showed a sustained release similar to that obtained by Jia et al.[23] In their study, doxorubicin-loaded PLGA-MNPs showed a burst release for the initial first day followed by sustained release for 7 days. This characteristic bi-phasic release was also observed in curcumin-loaded Alendronate-coated PLGA NPs for active targeting of breast cancer.[17]

Following the physical and chemical characterization of our R11-NU7441 NPs, *in vitro* studies were carried out to study cytocompatibility and cellular uptake in the presence or absence of a magnet. Greater than 80% PZ-HPV-7 viability was observed when incubated with all NP concentrations, which is in agreement with previous studies demonstrating the cytocompatibility of PLGA NPs with LAG mouse fibroblast connective tissue [24] and 3T3 fibroblasts.[25] Additionally, dose-dependent cellular uptake of our NPs by PC3 cells was observed, similar to observations by Akbarzadeh et al. [26] and Davda et al. [27] using Folate-PLGA-PEG NPs. The significantly higher magnetic-field dependent uptake of our particles by PC3 cells agrees with results obtained by Wadajkar et al., [28] where their biodegradable photoluminescent polymer (BPLP)-coated iron oxide NPs were also significantly uptaken by PC3 in the presence of a 1.3T magnet. The R11 conjugation onto the surface of our NPs also played a key role in active targeting and uptake of NU7441-loaded particles by prostate cancer cells. Our results concur with studies by Patel et al. [29] which showed higher dose-dependent uptake of R11-conjugated PLGA NPs by PC3 cells when compared to NPs conjugated with folic acid and RGD-4C.

Previously, we have demonstrated preferential uptake of R11 peptide by the prostate cancer cells and prostate tissues.[30,31] In addition, Hao et al.[30] performed a comparative PET-CT imaging experiment by using prostate (PC3) and lung (H2009) tumor-bearing mouse models and confirmed that the absolute uptake of ^{64}Cu-DOTA-NHGR11 in the PC3 tumors was significantly higher than in the lung (H2009) tumors throughout the imaging study. Using the colony formation assays, we show that R11-NU7441 NPs radiosensitize only prostate cancer cell lines. Furthermore, this enhanced radiation sensitivity in prostate cancer cells can be attributed to slower rate in DNA DSB break repair process due to the preferential uptake of R11-NU7441 NPs in prostate cancer cells.

In addition to the targeted delivery of radiosensitizers to prostate cancer cells presented in this work, NPs encapsulating radiosensitizers have also been used for other various cancer cells. For example, HeLa and MCF-7 have been successfully radiosensitized using PLGA NPs containing the hypoxic radiosensitizer etanidazole (SR-2508).[6] Similarly, PLGA NPs loaded with paclitaxel, which acts as both an anti-cancer drug as well as a radiosensitizer, has been effectively used *in vitro* against MCF-7 cells.[32] Also PLGA NPs containing curcumin have been developed and effectively used for chemoradiation sensitization of A2780CP ovarian cells.[33] However to the authors' knowledge, there have been no attempts so far to synthesize NPs for prostate cancer-specific active targeting and imaging *in vivo* as well as for providing a sustained release of a potent radiosensitizer for treatment of localized prostate cancer. This paper demonstrates that R11- conjugation on our NPs provides localized therapy. The R11 specifically targets the laminin receptor on prostate cancer cells resulting in a comparatively higher uptake of the NPs by these cells, compared to other cells in the body. The sustained release of encapsulated NU7441 from the PLGA NPs over time prevents DSB repair within the prostate cancer cells thus sensitizing them to radiation. Incorporation of imaging agents such as iron oxide assists in NP tracking and imaging using MRI as well as magnetic targeting to the cancer site using an external magnet. Therefore, the combination of PLGA NPs conjugated with R11 peptides and containing NU7441 radiosensitizer along with a suitable imaging agent would be beneficial in comparatively accurate tracking, targeting and imaging of the NPs as well as in effective radiosensitization of prostate cancer cells.

5. CONCLUSIONS

In this work, we have synthesized R11-conjugated PLGA-based NPs encapsulating NU7441 for targeted radiation sensitization of prostate cancer cells. The particles were stable and cytocompatible with a sustained NU7441 release profile for a period of 21 days. Additionally, the PC3 prostate cancer cells showed dose- and magnetic-dependent cellular uptake of our particles. The particles also showed good targeting capabilities *in vitro* by specifically inhibiting DNA DSB repair kinetics of PC3 cells while not affecting the H460 cells. While these particles require further testing, they have demonstrated a great potential for clinical application of radiation sensitizing strategy by sustained release of the NU7441 over time thus improving its solubility and bioavailability. Future studies will involve testing the radiosensitizing capabilities of the R11-NU7441 NPs *in vivo* in prostate tumor-bearing animals.

6. ACKNOWLEDGEMENTS

The authors acknowledge the UT Southwestern Imaging Core Facility and Dr. Jiechao Jiang at the Materials Science Department at The University of Texas at Arlington for the use of their instruments. We also thank Ms. Alicia J. Sisemore for her help with the manuscript editing.

7. REFERENCES

1. Siegel R, Ma J, Zou Z, Jemal A. Cancer statistics, 2014. CA: A Cancer Journal for Clinicians 2014;64(1):9-29.
2. Bolderson E, Richard DJ, Zhou B-BS, Khanna KK. Recent advances in cancer therapy targeting proteins Involved in DNA double-strand break repair. Clinical Cancer Research 2009;15(20):6314-6320.
3. Leahy JJ, Golding BT, Griffin RJ, Hardcastle IR, Richardson C, Rigoreau L, Smith GC. Identification of a highly potent and selective DNA-dependent protein kinase (DNA-PK) inhibitor (NU7441) by screening of chromenone libraries. Bioorg Med Chem Lett 2004;14(24):6083-7.
4. Zhao Y, Thomas HD, Batey MA, Cowell IG, Richardson CJ, Griffin RJ, Calvert AH, Newell DR, Smith GC, Curtin NJ. Preclinical evaluation of a potent novel DNA-dependent protein kinase inhibitor NU7441. Cancer research 2006;66(10):5354-5362.

5. Roa W, Zhang X, Guo L, Shaw A, Hu X, Xiong Y, Gulavita S, Patel S, Sun X, Chen J and others. Gold nanoparticle sensitize radiotherapy of prostate cancer cells by regulation of the cell cycle. Nanotechnology 2009;20(37):375101.
6. Jin C, Bai L, Wu H, Teng Z, Guo G, Chen J. Cellular uptake and radiosensitization of SR-2508 loaded PLGA nanoparticles. J Nanopart Res 2008;10(6):1045-1052.
7. Makadia HK, Siegel SJ. Poly lactic-co-glycolic acid (PLGA) as biodegradable controlled drug delivery carrier. Polymers 2011;3(3):1377-1397.
8. Jordan A, Scholz R, Wust P, FÃ¤hling H, Roland F. Magnetic fluid hyperthermia (MFH): Cancer treatment with AC magnetic field induced excitation of biocompatible superparamagnetic nanoparticles. Journal of Magnetism and Magnetic Materials 1999;201(1â€“3):413-419.
9. Laurent S, Forge D, Port M, Roch A, Robic C, Vander Elst L, Muller RN. Magnetic Iron Oxide Nanoparticles: Synthesis, Stabilization, Vectorization, Physicochemical Characterizations, and Biological Applications. Chemical Reviews 2008;108(6):2064-2110.
10. Hsieh J-T, Zhou J, Gore C, Zimmern P. R11, a novel cell-permeable peptide, as an intravesical delivery vehicle. BJU International 2011;108(10):1666-1671.
11. Zhou J, Fan J, Hsieh JT. Inhibition of mitogen-elicited signal transduction and growth in prostate cancer with a small peptide derived from the functional domain of DOC-2/DAB2 delivered by a unique vehicle. Cancer Res 2006;66(18):8954-8.
12. Wadajkar AS, Menon JU, Tsai YS, Gore C, Dobin T, Gandee L, Kangasniemi K, Takahashi M, Manandhar B, Ahn JM and others. Prostate cancer-specific thermo-responsive polymer-coated iron oxide nanoparticles. Biomaterials 2013;34(14):3618-25.
13. Rahimi M, Wadajkar A, Subramanian K, Yousef M, Cui W, Hsieh JT, Nguyen KT. In vitro evaluation of novel polymer-coated magnetic nanoparticles for controlled drug delivery. Nanomedicine 2010;6(5):672-80.
14. Anand P, Nair HB, Sung B, Kunnumakkara AB, Yadav VR, Tekmal RR, Aggarwal BB. Design of curcumin-loaded PLGA nanoparticles formulation with enhanced cellular uptake, and increased bioactivity in vitro and superior bioavailability in vivo. Biochemical Pharmacology 2010;79(3):330-338.
15. Hasan W, Chu K, Gullapalli A, Dunn SS, Enlow EM, Luft JC, Tian S, Napier ME, Pohlhaus PD, Rolland JP and others. Delivery of multiple siRNAs using lipid-coated PLGA nanoparticles for treatment of prostate cancer. Nano Letters 2012;12(1):287-292.
16. Jin C, Bai L, Wu H, Tian F, Guo G. Radiosensitization of paclitaxel, etanidazole and paclitaxel+etanidazole nanoparticles on hypoxic human tumor cells in vitro. Biomaterials 2007;28(25):3724-3730.
17. Thamake SI, Raut SL, Gryczynski Z, Ranjan AP, Vishwanatha JK. Alendronate coated poly-lactic-co-glycolic acid (PLGA) nanoparticles for active targeting of metastatic breast cancer. Biomaterials 2012;33(29):7164-7173.
18. Wadajkar AS, Bhavsar Z, Ko C-Y, Koppolu B, Cui W, Tang L, Nguyen KT. Multifunctional particles for melanoma-targeted drug delivery. Acta Biomaterialia 2012;8(8):2996-3004.
19. Okassa LN, Marchais H, Douziech-Eyrolles L, Herve K, Cohen-Jonathan S, Munnier E, Souce M, Linassier C, Dubois P, Chourpa I. Optimization of iron oxide nanoparticles encapsulation within poly(d,l-lactide-co-glycolide) sub-micron particles. Eur J Pharm Biopharm 2007;67(1):31-38.

20. Cheng F-Y, Su C-H, Yang Y-S, Yeh C-S, Tsai C-Y, Wu C-L, Wu M-T, Shieh D-B. Characterization of aqueous dispersions of Fe3O4 nanoparticles and their biomedical applications. Biomaterials 2005;26(7):729-738.
21. Xu C, Xu K, Gu H, Zhong X, Guo Z, Zheng R, Zhang X, Xu B. Nitrilotriacetic acid-modified magnetic nanoparticles as a general agent to bind Histidine-tagged proteins. Journal of the American Chemical Society 2004;126(11):3392-3393.
22. Menon JU, Kona S, Wadajkar AS, Desai F, Vadla A, Nguyen KT. Effects of surfactants on the properties of PLGA nanoparticles. J Biomed Mater Res A 2012;100(8):1998-2005.
23. Jia Y, Yuan M, Yuan H, Huang X, Sui X, Cui X, Tang F, Peng J, Chen J, Lu S and others. Co-encapsulation of magnetic Fe3O4 nanoparticles and doxorubicin into biodegradable PLGA nanocarriers for intratumoral drug delivery. Int J Nanomedicine 2012;7:1697-708.
24. Mathew A, Fukuda T, Nagaoka Y, Hasumura T, Morimoto H, Yoshida Y, Maekawa T, Venugopal K, Kumar DS. Curcumin loaded-PLGA nanoparticles conjugated with Tet-1 peptide for potential use in Alzheimer's disease. PLoS One 2012;7(3):e32616.
25. Moraes CM, de Matos AP, de Lima R, Rosa AH, de Paula E, Fraceto LF. Initial development and characterization of PLGA nanospheres containing ropivacaine. J Biol Phys 2007;33(5-6):455-61.
26. Akbarzadeh A, Mikaeili H, Zarghami N, Mohammad R, Barkhordari A, Davaran S. Preparation and in vitro evaluation of doxorubicin-loaded Fe(3)O(4) magnetic nanoparticles modified with biocompatible copolymers. Int J Nanomedicine 2012;7:511-26.
27. Davda J, Labhasetwar V. Characterization of nanoparticle uptake by endothelial cells. Int J Pharm 2002;233(1-2):51-9.
28. Wadajkar AS, Kadapure T, Zhang Y, Cui W, Nguyen KT, Yang J. Dual-imaging enabled cancer-targeting nanoparticles. Adv healthcare mater 2012;1(4):450-456.
29. Patel RH, Wadajkar AS, Patel NL, Kavuri VC, Nguyen KT, Liu H. Multifunctionality of indocyanine green-loaded biodegradable nanoparticles for enhanced optical imaging and hyperthermia intervention of cancer. J Biomed Opt 2012;17(4):046003.
30. Hao G, Zhou J, Guo Y, Long MA, Anthony T, Stanfield J, Hsieh JT, Sun X. A cell permeable peptide analog as a potential-specific PET imaging probe for prostate cancer detection. Amino Acids 2010.
31. Zhou J, Liu W, Pong RC, Hao G, Sun X, Hsieh JT. Analysis of oligo-arginine cell-permeable peptides uptake by prostate cells. Amino Acids 2010.
32. Jin C, Wu H, Liu J, Bai L, Guo G. The effect of paclitaxel-loaded nanoparticles with radiation on hypoxic MCF-7 cells. Journal of Clinical Pharmacy and Therapeutics 2007;32(1):41-47.
33. Yallapu MM, Maher DM, Sundram V, Bell MC, Jaggi M, Chauhan SC. Curcumin induces chemo/radio-sensitization in ovarian cancer cells and curcumin nanoparticles inhibit ovarian cancer cell growth. J Ovarian Res 2010;3:11.

Figure Legends

Fig. 1. (A) TEM image representing spherical PLGA-iron oxide nanoparticles (~260 nm) with iron oxide present on the core and surface of the particles. **(B)** Photographs demonstrating the recruitment of the R11-NU7441 NPs towards a 1.3T external magnet. **(C)** FTIR spectra indicating successful conjugation of R11 and incorporation of iron oxide onto the NPs. **(D)** Comparison of hysteresis loops of R11-NU7441 NPs and bare MNPs demonstrating the existence of superparamagnetic behavior of both in the presence of a magnetic field.

Fig. 2. Comparison of stability of R11-NU7441 NPs in DI water and 10% FBS showing no significant change in particle size for 5 days at 37^{o}C thus demonstrating that the NPs are stable and do not aggregate in these solutions (n=4).

Fig. 3. NU7441 release profile from the NPs demonstrating a bi-phasic release which includes initial burst release of 41% of NU7441 within 1 day followed by sustained release for 3 weeks (n=4).

Fig. 4. (A) Cell viability study showed that the R11-NU7441 NPs were cytocompatible up to a concentration of 1000 µg/ml with more than 80% cell viability noticed at all concentrations (n=4, *p<0.05 w.r.t. control). **(B)** Cellular uptake of unconjugated NPs in the presence of a 1.3T external magnet. Uptake of R11-conjugated NPs in the presence (1.3T) and absence (0 T) of an external magnet and at varying NP concentrations showing dose- and magnetic field-dependence of cellular uptake of these NPs (n=4, *p <0.05 w.r.t. R11-NU7441 NP uptake, #p <0.05 w.r.t. uptake of unconjugated NPs).

Fig. 5. DNA DSB repair kinetics in **(A)** lung cancer (H460) and **(B)** prostate (WT PC3) cells using radiation therapy (RT) (Blue Bar), R11-NU7441 NPs (Red Bar) and R11 NPs (control particle, Green Bar). Cells were treated as indicated and washed before RT (2 Gy). Samples were collected at the indicated time points stained with H2AX foci. Foci counts represent the average of at least 100 nuclei.

Fig. 6. Surviving fraction analysis using R11-NU7441 NPs. **(A)** H460 cells as well as **(B)** PC3 cells were treated with increasing dosages of NPs followed by treatment with radiation as indicated.

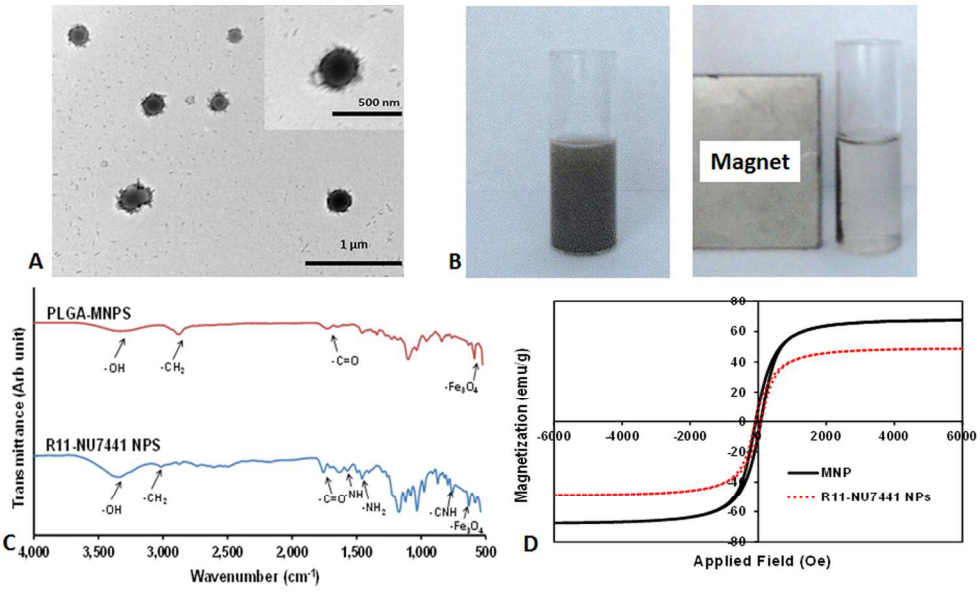

Fig. 1. (A) TEM image representing spherical PLGA-iron oxide nanoparticles (~260 nm) with iron oxide present on the core and surface of the particles. (B) Photographs demonstrating the recruitment of the R11-NU7441 NPs towards a 1.3T external magnet. (C) FTIR spectra indicating successful conjugation of R11 and incorporation of iron oxide onto the NPs. (D) Comparison of hysteresis loops of R11-NU7441 NPs and bare MNPs demonstrating the existence of superparamagnetic behavior of both in the presence of a magnetic field.
76x44mm (600 x 600 DPI)

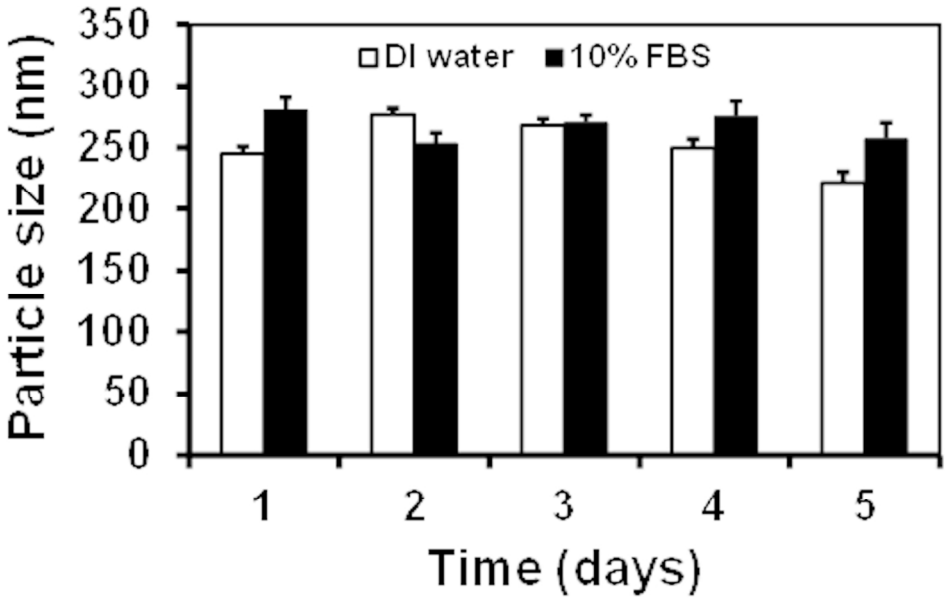

Fig. 2. Comparison of stability of R11-NU7441 NPs in DI water and 10% FBS showing no significant change in particle size for 5 days at 37oC thus demonstrating that the NPs are stable and do not aggregate in these solutions (n=4).
63x38mm (600 x 600 DPI)

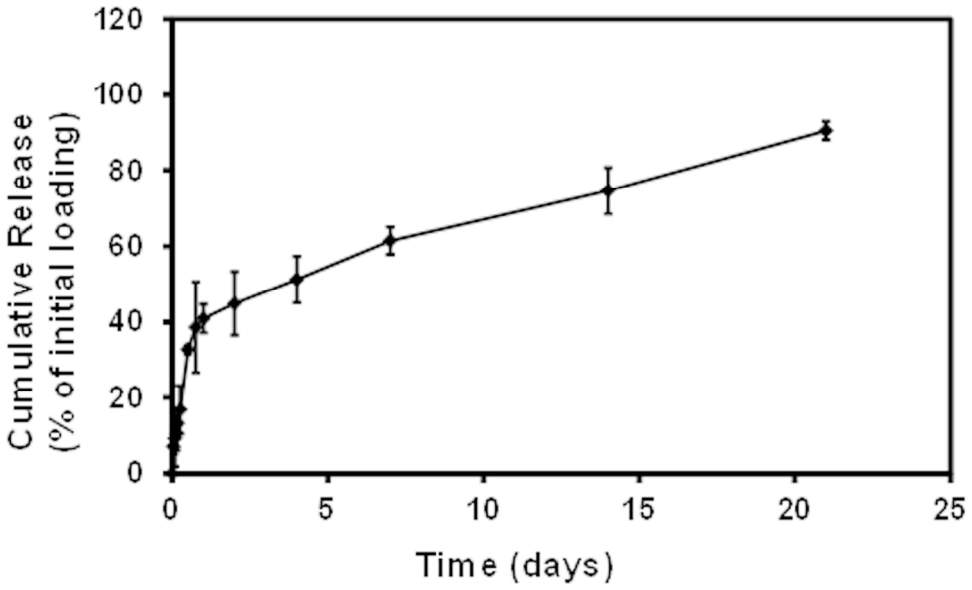

Fig. 3. NU7441 release profile from the NPs demonstrating a bi-phasic release which includes initial burst release of 41% of NU7441 within 1 day followed by sustained release for 3 weeks (n=4).
76x46mm (600 x 600 DPI)

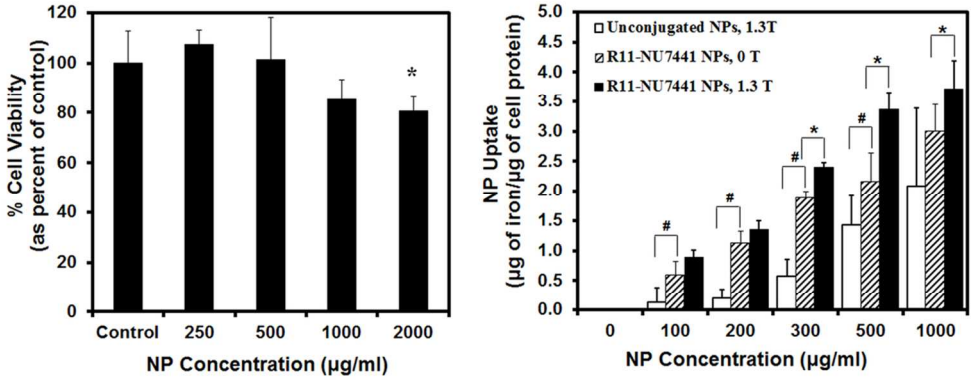

Fig. 4. (A) Cell viability study showed that the R11-NU7441 NPs were cytocompatible up to a concentration of 1000 µg/ml with more than 80% cell viability noticed at all concentrations (n=4, *p<0.05 w.r.t. control). (B) Cellular uptake of unconjugated NPs in the presence of a 1.3T external magnet. Uptake of R11-conjugated NPs in the presence (1.3T) and absence (0 T) of an external magnet and at varying NP concentrations showing dose- and magnetic field-dependence of cellular uptake of these NPs (n=4, *p <0.05 w.r.t. R11-NU7441 NP uptake, #p <0.05 w.r.t. uptake of unconjugated NPs).
53x20mm (600 x 600 DPI)

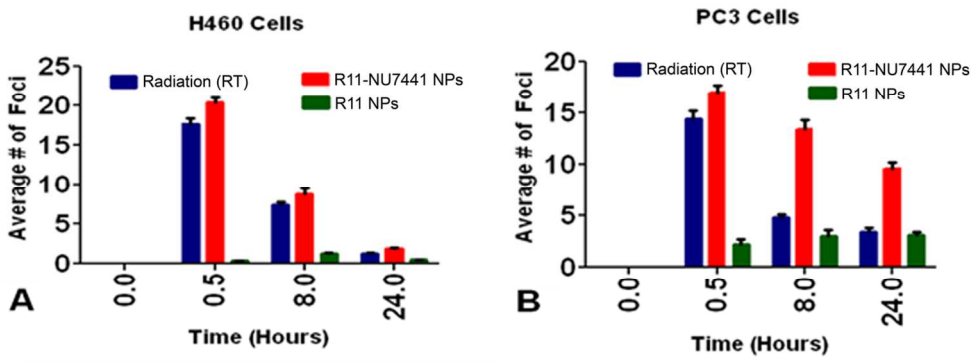

Fig. 5. DNA DSB repair kinetics in (A) lung cancer (H460) and (B) prostate (WT PC3) cells using radiation therapy (RT) (Blue Bar), R11-NU7441 NPs (Red Bar) and R11 NPs (control particle, Green Bar). Cells were treated as indicated and washed before RT (2 Gy). Samples were collected at the indicated time points stained with H2AX foci. Foci counts represent the average of at least 100 nuclei.
59x21mm (600 x 600 DPI)

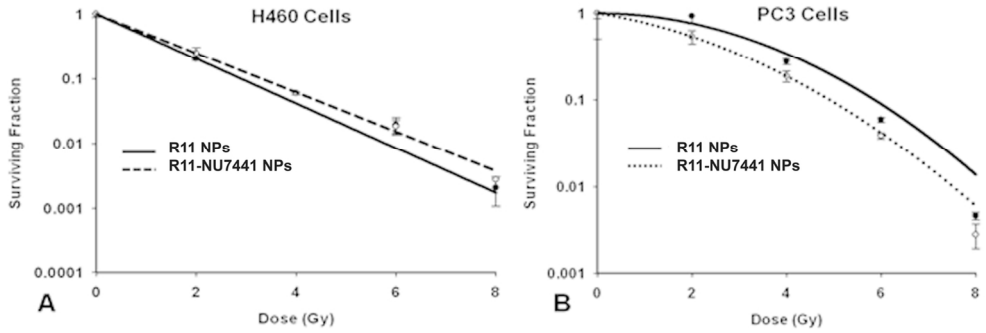

Fig. 6. Surviving fraction analysis using R11-NU7441 NPs. (A) H460 cells as well as (B) PC3 cells were treated with increasing dosages of NPs followed by treatment with radiation as indicated.
63x23mm (600 x 600 DPI)